

Diurnal variations of resting-state fMRI data: A graph-based analysis

Farzad V. Farahani^{1*}, Waldemar Karwowski¹, Mark D'Esposito^{2,3}, Richard F. Betzel⁴, Magdalena Fafrowicz^{5*}, Bartosz Bohaterewicz⁵, Tadeusz Marek⁵, Pamela K. Douglas^{6,7}

¹Computational Neuroergonomics Laboratory, Department of Industrial Engineering and Management Systems, University of Central Florida, Orlando, FL, USA

²Helen Wills Neuroscience Institute, University of California, Berkeley, CA, USA

³Department of Psychology, University of California, Berkeley, CA, USA

⁴Department of Psychological and Brain Sciences, Indiana University, Bloomington, IN, USA

⁵Department of Cognitive Neuroscience and Neuroergonomics, Institute of Applied Psychology, Jagiellonian University, Kraków, Poland

⁶Institute for Simulation and Training, University of Central Florida, Orlando, FL, USA

⁷Department of Psychiatry and Biobehavioral Sciences, University of California, Los Angeles, Los Angeles, CA, USA

*** Correspondence:**

Farzad V. Farahani

farzad.vasheghani@knights.ucf.edu

Magdalena Fafrowicz

magda.fafrowicz@uj.edu.pl

Keywords: functional connectivity, resting state-fMRI, graph theory, diurnal (circadian) rhythm, morning and evening chronotypes, small-world, brain networks.

Abstract

Circadian rhythms (lasting approximately 24 hours) control and entrain a variety of physiological processes ranging from neural activity and hormone secretion to sleep cycles and feeding habits. Despite significant diurnal variation in human brain function, neuroscientists have rarely considered the effects of time-of-day (TOD) on their studies. Moreover, there are inter-individual discrepancies in sleep-wake patterns, diurnal preferences, and daytime alertness (known as chronotypes), which could be associated with human cognition and brain performance. In the present study, we performed graph-theory based network analysis on resting-state functional MRI (rs-fMRI) data to explore the topological differences in whole-brain functional networks between the morning and evening sessions (TOD effect), as well as between extreme morning-type and evening-type participants (chronotype effect). To that end, 62 individuals (31 extreme morning-versus 31 evening-type) underwent two fMRI sessions: about 1 hour after the wake-up time (morning) and about 10 hours after the wake-up time (evening), scheduled in accord with their declared habitual sleep-wake pattern on a regular working day. The findings revealed the significant effect of TOD on the functional connectivity (FC) patterns, but there was no significant difference in chronotype categories. Compared to the morning session, we found relatively increased small-worldness, modularity, assortativity, and synchronization in the evening session, indicating more efficient functional topology. Local measures were changed during the day predominantly across the areas involved in somatomotor, ventral attention, as well as default mode networks. Also, connectivity and hub analyses showed that the somatomotor, ventral attention, and visual networks are the most densely-connected brain areas in both sessions, respectively, with the first being more active in the evening session and the two latter in the morning session. Finally, we performed a correlation analysis to examine whether network properties are associated with the subjective assessments across subjects, most of which happened in the morning session. All these findings contribute to an increased understanding of diurnal fluctuations in resting neural activity and highlight the role of TOD in future brain studies.

Keywords: sleep, chronotype, graph theory, small world, fMRI, functional connectivity

1. Introduction

Circadian rhythms are natural, internal ~24-hour fluctuations in most living organisms, regulating a variety of physiological functions, including sleep-wake patterns (Borbély, 1982; Dijk and Lockley, 2002; Schmidt et al., 2012), body temperature (Refinetti and Menaker, 1992), endocrine and metabolic rhythms (Hastings et al., 2007), gene expression (Storch et al., 2002), musculoskeletal activity (Aoyama and Shibata, 2017), as well as a wide range of brain functions (Schmidt et al., 2007). Studies of brain function in humans have shown circadian variations in a wide variety of abilities such as attention (Valdez et al., 2005), working memory (Ramírez et al., 2006), motor (Edwards et al., 2007) and visual detection (Tassi et al., 2000). These studies have investigated function at multiple scales of brain organization from that of individual cells and synapses (Gilestro et al., 2009; Kuhn et al., 2016; Vyazovskiy et al., 2008) to brain regions and large-scale FC (Blautzik et al., 2013; Hodkinson et al., 2014; Orban et al., 2020; Shannon et al., 2013; Steel et al., 2019).

A chronotype is a biologically driven circadian typology that generally refers to the individual differences in sleep-wake cycles, diurnal preferences, and alertness throughout the day (Roenneberg et al., 2003; Susman et al., 2007). Traditionally, individuals fall into morning (“early larks”) or evening (“night owls”) chronotypes. Evening chronotypes typically have phases of behavioral and physiological circadian clocks shifted toward later hours than morning chronotypes (Bailey and Heitkemper, 2001; Kerkhof and Dongen, 1996). Various studies have shown that people with different chronotypes have significantly different diurnal profiles of cognition and behavior (Horne et al., 1980; Norbury, 2020; Schmidt et al., 2007; Valdez et al., 2012). Also, circadian variations in performance-related neural activity have been reported in studies utilizing chronotype-based paradigms (e.g., Facer-Childs et al., 2019; Fafrowicz et al., 2009; Gorfine et al., 2007; Peres et al., 2011; Schmidt et al., 2009, 2012, 2015; Vandewalle et al., 2009, 2011).

However, there have been a limited number of resting-state and task-based functional MRI studies investigating the impact of both TOD and chronotype on behavior, cognition, and neural activity (Blautzik et al., 2013; Cordani et al., 2018; Hodkinson et al., 2014; Jiang et al., 2016; Shannon et al., 2013; Steel et al., 2019; Gorfine and Zisapel, 2009; Marek et al., 2010), often yielding contradictory or sometimes even ambiguous findings. Also, most fMRI studies assume that diurnal fluctuations of brain connectivity patterns as well as human chronotypes are relatively insignificant and are unlikely to lead to a substantial systematic bias into group analysis (Orban et al., 2020).

Here, we examined the effect of TOD on the rs-fMRI data, taking into account subject chronotype, using methodology from network neuroscience. To this end, we directly compared the topological changes (global and local) in FC patterns between morning and evening sessions, as well as the network properties across early larks and night owls. In global analysis, we found a more efficient functional topology as the waking time increased, and local analysis showed significant changes mostly in the somatomotor, ventral attention, and default mode networks. However, we did not find any compelling evidence of the chronotype effect on the network topology itself. Within the context of these findings, it is clear that TOD may influence connectivity patterns in resting state fMRI data, making this variable an potentially important factor to consider in future rs-fMRI experiments.

2. Materials and methods

2.1. Participants and study procedures

Participants were recruited through online advertisements on the lab's website and Facebook. 5354 volunteers participated in the first stage of selection and were asked to complete two questionnaires: the Chronotype Questionnaire (Oginska et al., 2017) for diurnal preferences assessment and the Epworth Sleepiness Scale (ESS; Johns, 1991) for daytime sleepiness measurements as well as the sleep-wake assessment (real versus ideal wake- and bedtimes). Individuals reporting excessive daytime sleepiness were excluded from the study, as determined by the cut-off points ESS (≤ 10 points) questionnaire. 451 participants were divided into morning or evening chronotypes and underwent PER3 VNTR polymorphism genotyping, isolated from buccal swabs using DNA GeneMATRIX Swab-Extract DNA Purification Kit (EURx, Gdańsk, Poland) following manufacturers protocol. Only subjects that were homozygous for the PER3 4 (ES) and PER3 5 (MS) alleles were included for the study. Other selection criteria included an age between 20 and 35 years, right-handed as indicated by the Edinburgh Handedness Inventory (Oldfield, 1971), regular TOD schedule without sleep debt, no neurological or psychiatric disorders, no addiction, normal or corrected-to-normal vision, and no MRI contraindications. Thus, 64 healthy and young participants (39 women, mean age: 23.97 ± 3.26 y.o.) were selected for the study that met these criteria.

Resting-state fMRI (rs-fMRI) was performed twice – in the morning (MS) and evening (ES) sessions – about one and ten hours after awakening from a night-time of sleep, respectively. Participants were asked to maintain a regular sleep-wake schedule one week before study, controlled using MotionWatch 8 actigraphs. These actigraphs were also worn during the study days for supervising subjects' sleep length and quality. Furthermore, the night before the morning session, subjects slept in rooms located in the same building where the MRI scanner was located. Individuals abstained from alcohol (48 h) and caffeine (24 h) before MRI scanning sessions and were only allowed to engage in non-strenuous activities during study days. The study was approved by the Institute of Applied Psychology Ethics Committee of the Jagiellonian University. Informed, written consent was provided by all participants in accordance with the Declaration of Helsinki. Demographics, questionnaires and actigraphy results are provided for the morning and evening chronotypes in the Table 1.

Table 1. Demographics, questionnaires and actigraphy results.

Variables (mean ± SD)	MT (N=31)	ET (N=31)	Sign.
Sex (M/F) ^a	11/20	12/19	ns
Age (years) ^b	24.45 ± 3.83	23.48 ± 2.55	ns
ME ^b	15.71 ± 2.41	28.45 ± 2.39	*
AM ^b	21.47 ± 3.58	22.26 ± 3.51	ns
ESS ^b	5.52 ± 2.48	5.87 ± 3.01	ns
EHI ^b	86.83 ± 12.92	89.19 ± 13.93	ns
VNTR of PER3	5/5	4/4	-
Declared waketime (hh:mm) ^c	07:07 ± 62 min	07:25 ± 48 min	ns
Declared bedtime (hh:mm) ^c	23:24 ± 55 min	00:06 ± 49 min	*
Declared length of perfect sleep (hh:mm) ^c	08:50 ± 42 min	08:38 ± 54 min	ns
Actigraphy-derived waketime (hh:mm) ^c	07:43 ± 70 min	08:16 ± 69 min	ns
Actigraphy-derived bedtime (hh:mm) ^c	23:58 ± 58 min	00:48 ± 58 min	*
Actigraphy-derived length of real sleep (hh:mm) ^c	07:53 ± 51 min	07:36 ± 40 min	ns

Abbreviations: *MT* morning types, *ET* evening types, *ME* morningness/eveningness scale (from Chronotype Questionnaire), *AM* amplitude scale (from Chronotype Questionnaire), *ESS* Epworth Sleepiness Scale, *EHI* Epworth Handedness Inventory, ^a chi-square test, ^b Mann-Whitney U test, ^c Student's t-test, * *p*-value < 0.05, *ns* non-significant.

2.2. Data acquisition

Magnetic resonance imaging was performed using a 3T Siemens Skyra MR System equipped with a 64-channel head coil. Anatomical images were obtained with the use of sagittal 3D T1-weighted MPRAGE sequence. Ten minutes of resting-state blood-oxygenation-level-dependent (BOLD) images were acquired using a gradient-echo single-shot echo planar imaging sequence with the following parameters: repetition time (TR) = 1,800 ms; echo time (TE) = 27 ms; field of view (FOV) = 256 × 256 mm²; slice thickness = 4 mm; voxel size = 4 × 4 × 4 mm³, with no gap. A total of 34 interleaved transverse slices and 335 volumes acquired in each participants. During scanning, participants were instructed to stay awake and keep their eyes open throughout the scanning session. No other task instruction was provided. Participants' were monitored using an eye tracking system to ensure they were awake throughout the duration of the scan (Eyelink 1000, SR research, Mississauga, ON, Canada).

2.3. Data preprocessing

Data preprocessing was performed using DPABI v. 4.2 and SPM 12 both working under Matlab v.2018a (The Mathworks Inc.). Due to the signal equilibration, first 10 time points were discarded. Subsequently, slice timing and realignment with assessment of voxel specific head motion were conducted. The subjects with movements in one or more of the orthogonal directions above 3 mm or rotation above 3° were discarded from the analysis. As the result, a total of four participants were excluded due to the excessive head movements. Then, functional scans were registered using T1 images and then to Montreal Neurological Institute (MNI) space using DARTEL and voxel size of 3 × 3 × 3 mm³. Altogether, seven participants were excluded due to the low quality of the image registration. The functional data was spatially smoothed with 4 mm Full Width at Half Maximum (FWHM) kernel. The 24 motion parameters, which were derived from the realignment step were regressed out from the functional data by linear regression as well as five principal

components from both cerebrospinal fluid and white matter signals using principal components analysis integrated in a Component Based Noise Correction Method (Behzadi et al., 2007). The global signal was included due to its potential in providing the additional valuable information (Liu et al., 2017) and the signal was band-pass filtered (0.01 – 0.1 Hz).

2.4. Brain network construction

A large-scale brain network consists of a finite set of nodes (brain regions) that are connected by links (FC between nodes). In this study, the nodes were specified by parcellation of the whole brain into 7 networks and 200 cortical ROIs from the Schaefer/Yeo atlas (Schaefer et al., 2018). One of the many advantages of this atlas is that each node is preassigned to a system/network (visual, somatomotor, dorsal attention, salience/ventral attention, limbic, frontoparietal, and default mode). The average BOLD time series across all voxels within each ROI were separately extracted. Then, the FC between each pair of ROIs was computed by means of Pearson's correlation coefficient. To improve the normality, the correlation values were converted into z values using Fisher's r-to-z transformation. At this stage, a symmetrical FC matrix (adjacency matrix) with a size of 200×200 was constructed for each subject. Given the controversy over the use of negative correlations (Schwarz and McGonigle, 2011; Wang et al., 2011), we confined the analysis to positive correlations and set the negative coefficients to zero. An overview of our analysis pipeline is shown in **Figure 1**.

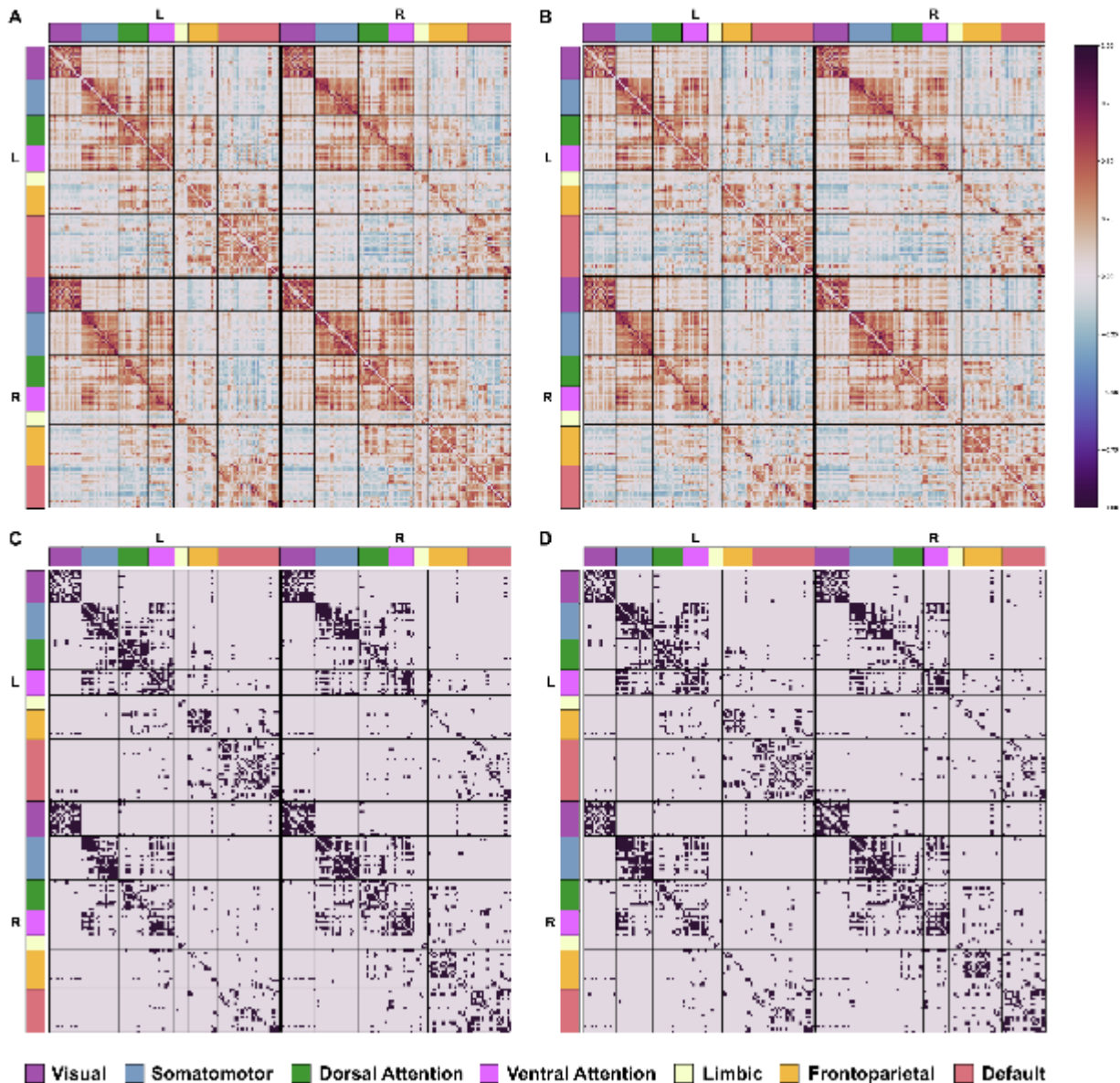


Figure 2. Weighted correlation matrices and binarized connectivity matrices (top 10% strongest connections) for both morning (A and C) and evening (B and D) sessions (averaged across all participants in each session).

2.5. Computation of graph metrics

Using binary undirected matrices, we examined the topological properties of functional brain networks for each participant (across a range of cost thresholds) at both global and local levels with the Brain Connectivity Toolbox (BCT¹; Rubinov and Sporns, 2010). Table 2 provides mathematical definitions and descriptive explanations of each network statistic. Global measures principally describe the functional segregation and integration of brain networks. Thus, we calculated global efficiency, modularity, mean clustering coefficient, characteristic path length, small-worldness, assortativity, and synchronization. Local measures of networks were calculated

¹ <http://www.brain-connectivity-toolbox.net/>

for each individual node (region) separately, examining the nodal centrality and density of network hubs (i.e., nodes with greater than average number of links). Hubs are generally divided into provincial (which mostly contain local connections within a module) and connector (which contain both local and long-range links to connect nodes in different modules). Thus, we calculated the most common local properties including degree centrality, betweenness centrality, nodal clustering coefficient, nodal efficiency, and participant coefficient (Rubinov and Sporns, 2010).

Table 2. Mathematical definition and explanation of measures used in this study (for binary and undirected graphs).

Description	Equation
<i>Degree (nodal)</i> : It computes the number of nodes neighbors (connections).	For a given node i , $k_i = \sum_{j \in N} a_{ij}$ N : Set of all nodes in the network.
<i>Path length (nodal)</i> : It quantifies the potential for information transmission and is determined as the average distance from a node to all other nodes. <i>Characteristic path length (global)</i> : Average of the path lengths of all other nodes.	Characteristic path length of the network (Watts and Strogatz, 1998), $L = \frac{1}{n} \sum_{i \in N} L_i = \frac{1}{n} \sum_{i \in N} \frac{\sum_{j \in N, j \neq i} d_{ij}}{n-1}$ n : Number of nodes. L_i : Average distance from node i to all other nodes (path length). d_{ij} : Shortest path length (distance) between nodes i and j .
<i>Efficiency (nodal)</i> : It computes the efficiency of parallel information transfer of a given node and is determined as the average of the inverse shortest path length from a node to all other nodes. <i>Efficiency (global)</i> : Average of the nodal efficiencies of all nodes.	Global efficiency of the network (Latora and Marchiori, 2001), $E = \frac{1}{n} \sum_{i \in N} E_i = \frac{1}{n} \sum_{i \in N} \frac{\sum_{j \in N, j \neq i} d_{ij}^{-1}}{n-1}$ E_i : Efficiency of node i .
<i>Clustering coefficient (nodal)</i> : The extent to which the neighbors of a given node are interconnected (i.e., fraction of triangles around a node). <i>Clustering coefficient (global)</i> : Average of the nodal clustering coefficients of all nodes. To achieve the clustering coefficient of a specific region, one can calculate the mean of the coefficients across that region.	Clustering coefficient of the network (Watts and Strogatz, 1998), $C = \frac{1}{n} \sum_{i \in N} C_i = \frac{1}{n} \sum_{i \in N} \frac{\sum_{j, k \in N} a_{ij} a_{ik} a_{jk}}{k_i(k_i - 1)}$ k_i : Degree of node i . a_{ij} is the connection between i and j : $a_{ij} = 1$ when link (i, j) exists, and 0 otherwise. There are no self-loops in the network, and therefore $a_{ii} = 0$.
<i>Modularity (global)</i> : It reflects clusters of densely interconnected nodes with sparse connections among other clusters.	Modularity of the network (Newman, 2004), $Q = \frac{1}{l} \sum_{i, j \in N} \left(a_{ij} - \frac{k_i k_j}{l} \right) \delta_{m_i, m_j}$ L : Set of all links in the network. $l = \sum_{i, j \in N} a_{ij}$: Number of links. m_i : The module containing node i , $\delta_{m_i, m_j} = 1$ if $m_i = m_j$, and 0 otherwise (assume that the given network consists of M non-overlapping modules).

<p><i>Small-worldness (global)</i>: It is dedicated to graphs in which most nodes are not neighbors but can be reached by any other node with the minimum possible path length. Small-world networks exhibit an intermediate balance between regular and random networks (i.e., they consist of many short-range links alongside a few long-range links), thus reflecting a high clustering coefficient and a short path length.</p>	<p>Small-worldness of the network (Humphries and Gurney, 2008),</p> $SW = \frac{C_{net}/C_{rand}}{L_{net}/L_{rand}}$ <p>C_{net} and L_{net} are clustering coefficient and path length of a given network, and C_{rand} and L_{rand} are these measures for an equivalent random network. Small-world networks often have $S \gg 1$.</p>
<p><i>Assortativity (global)</i>: The extent to which a network can resist failures in its main components.</p> <p>If $r \geq 0$, the nodes with high degree are more likely to connect to others that are similar in degree (an assortative network), while $r < 0$ reflects that high-degree nodes tend to attach to nodes with low degree (a disassortative network).</p>	<p>Assortativity coefficient of the network (Newman, 2002),</p> $r = \frac{\frac{1}{T} \sum_{(i,j) \in L} k_i k_j - \left[\frac{1}{T} \sum_{(i,j) \in L} \frac{1}{2} (k_i + k_j) \right]^2}{\frac{1}{T} \sum_{(i,j) \in L} \frac{1}{2} (k_i^2 + k_j^2) - \left[\frac{1}{T} \sum_{(i,j) \in L} \frac{1}{2} (k_i + k_j) \right]^2}$
<p><i>Synchronization (global)</i>: It examines how network nodes fluctuate in the same wave pattern.</p>	<p>Synchronization of the network (Barahona and Pecora, 2002),</p> $S = \frac{\lambda(2)}{\lambda(M)}$ <p>$\lambda(2)$: Second smallest eigenvalue of the matrix of A. $\lambda(M)$: Largest eigenvalue of the matrix of A A: Adjacent matrix of the network.</p>
<p><i>Betweenness centrality (nodal)</i>: The ratio of all shortest paths in the network that contain a given node.</p>	<p>Betweenness centrality of node i (Freeman, 1978),</p> $BC_i = \frac{1}{(n-1)(n-2)} \sum_{\substack{h,j \in N \\ h \neq j, h \neq i, j \neq i}} \frac{\rho_{hj}(i)}{\rho_{hj}}$ <p>ρ_{hj}: Number of shortest paths between h and j. $\rho_{hj}(i)$: Number of shortest paths between h and j that use i.</p>
<p><i>Participation coefficient (nodal)</i>: The distribution of a node's connections across its communities.</p>	<p>Participation coefficient of node i (Guimerà and Nunes Amaral, 2005),</p> $P_i = 1 - \sum_{m \in M} \left(\frac{k_i(m)}{k_i} \right)^2$ <p>M: Set of non-overlapping modules. $k_i(m)$: Number of links between i and all nodes in module m.</p>

Adopted from: <https://sites.google.com/site/bctnet/measures>.

2.6. Statistical analyses

We applied a non-parametric permutation test (p -values were calculated from 50,000 permutations) to investigate the significance of variations and correlations, which does not require any distributional assumptions (Nichols and Holmes, 2002). Also, FDR correction was applied to all statistical tests conducted in this manuscript.

3. Results

3.1. Global properties

Among the global measures examined, significant differences were found in the small-worldness, network synchronization, and assortativity between morning and evening sessions (**Figure 3**). No compelling evidence of changes was found in other global measures. Small-worldness (**Figure**

3A) decreased with higher network sparsity in both sessions. Compared to the morning session, the evening session showed higher small-worldness at sparsity 0.05 and 0.1 ($p < 0.05$, FDR corrected), which did not differ between chronotypes. Assortativity (**Figure 3B**) and network synchronization (**Figure 3C**) increased with higher network sparsity in both sessions. Contrast analysis showed that the assortativity and synchronization were significantly higher during the evening session than the morning session at sparsity 0.3 to 0.5 ($p < 0.05$, FDR corrected), which did not differ between chronotypes.

There were also significant differences in the modularity index between the two sessions at lower sparsity ($p < 0.05$, FDR corrected; **Figure 4**). Modularity was higher in the evening session as compared to the morning session.

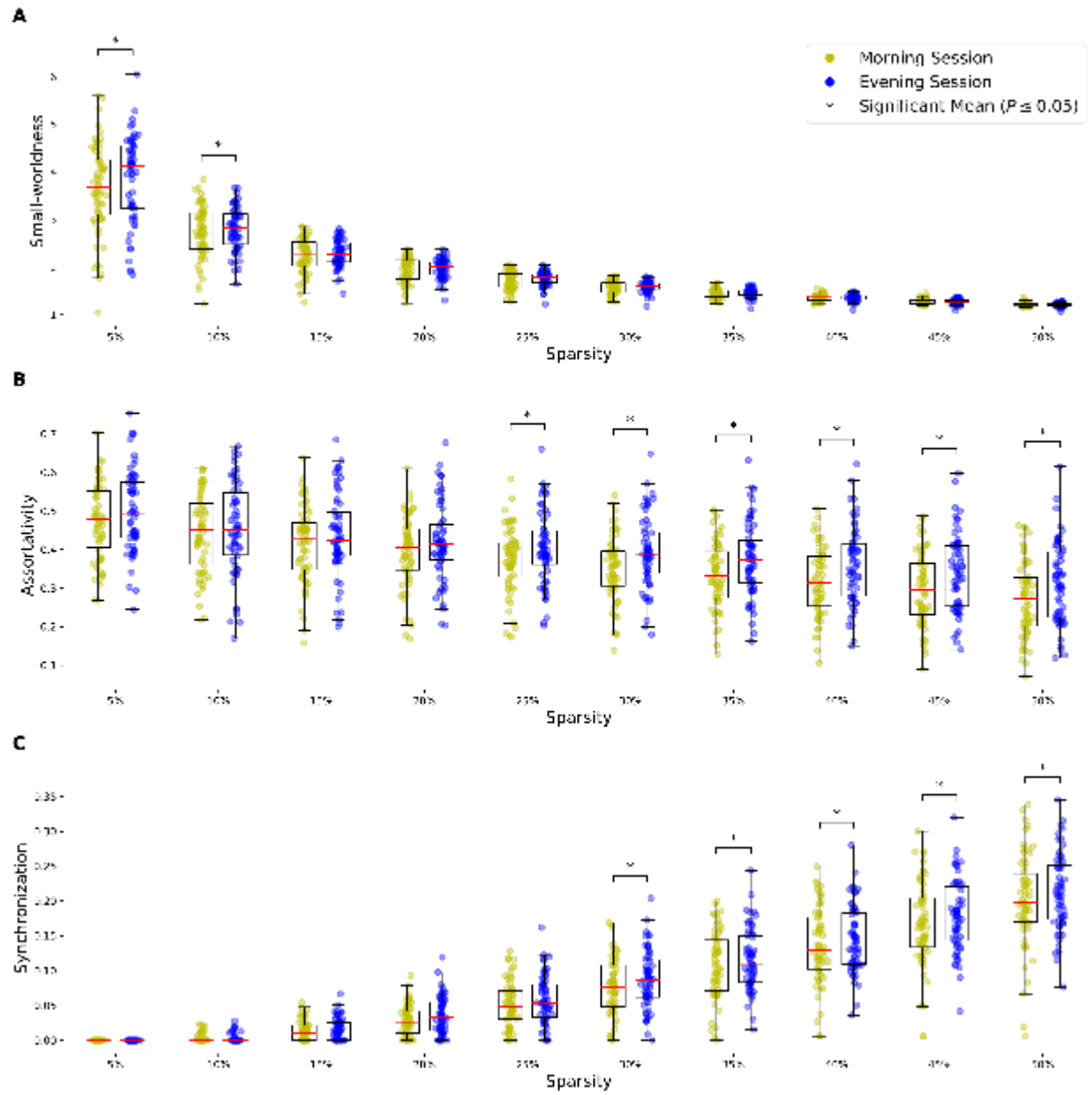


Figure 3. Differences of the small-worldness (A), assortativity (B) and synchronization (C) between the morning and evening sessions at the threshold values of 0.05 to 0.5 (p -values were computed using 50,000 permutations).

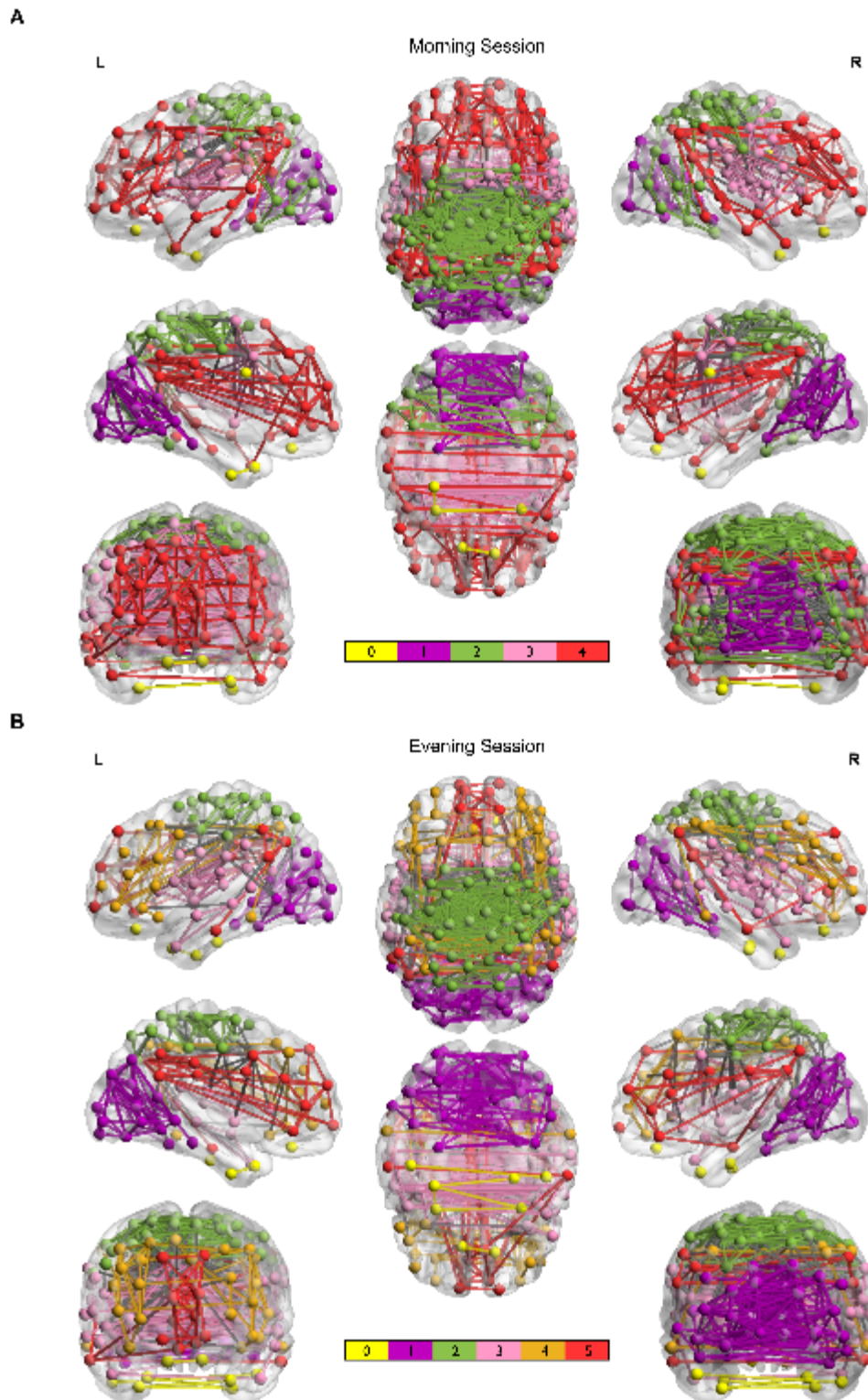


Figure 4. Modular brain network of the morning session and the evening session at a sparsity of 0.05 (visualization is based on the group-averaged data, while statistical analyses were carried out using individual subjects). There were four modules in the morning session (A) and five modules in the evening session (B). The horizontal color bar indicates the color coding of the modules (non-assigned nodes are marked with zero). Node connections within each module are represented in the module's color, while connections between different modules are represented in gray.

3.2. Local properties

Table 3 summarizes brain regions that significantly changed throughout the day using a set of nodal/local properties. The areas under the curve (AUC) were calculated for each network measure to provide a scalar that does not depend on a specific threshold selection (Wang et al., 2009; Zhang et al., 2011). As presented in **Table 3**, we found significant differences between the morning and evening sessions in terms of their degree centrality, betweenness centrality, clustering coefficient, and nodal efficiency. Most of these differences involved regions and their homotopic partners in the opposite hemisphere. No significant differences in participation coefficient and nodal shortest path were found between the two sessions ($p > 0.05$).

The AUC analysis for degree centrality, betweenness centrality, clustering coefficient, and nodal efficiency for all 200 brain regions are presented in **Figure 5**. Compared with the morning session, the evening session showed significantly increased degree centrality in the left somatomotor network and areas such as the superior temporal gyrus and postcentral gyrus, and decreased degree centrality in the left ventral attention and control network and areas such as supramarginal, middle frontal, and angular gyri ($p < 0.05$, FDR corrected). Similar results to degree centrality were obtained for the nodal efficiency. Betweenness centrality analysis also showed a significant increase in the evening session compared to the morning session in areas such as the bilateral precuneous, right postcentral gyrus, and right superior parietal gyrus. Finally, nodal clustering coefficient was increased in the evening session as compared to the morning session in the left dorsal anterior cingulate gyrus and right temporal gyrus (middle and superior), while it was decreased in the right angular gyrus over the course of the day.

Table 3. List of brain ROIs that significantly changed throughout the day (p -values were computed using 50,000 permutations followed by FDR correction).

ROI	Schaefer node label	Cortical areas	MNI coordinates			Adjusted p -value			
			x	y	z	Degree Centrality	Betweenness Centrality	Clustering Coefficient	Nodal Efficiency
15	LH_SomMot_1	L_Superior temporal gyrus	-51	-4	-2	0.0053			0.0069
16	LH_SomMot_2	L_Superior temporal gyrus	-53	-24	9	0.0132			0.0164
25	LH_SomMot_11	L_Superior parietal gyrus	-31	-46	63	0.0287			0.0234
30	LH_SomMot_16	L_Postcentral gyrus	-19	-31	68	0.0056			0.0075
46	LH_SalVentAttn_ParOper_3	L_Supramarginal gyrus	-60	-39	36	0.0250			0.0297
51	LH_SalVentAttn_PFC1_1	L_Middle frontal gyrus (dorsal prefrontal cortex)	-28	43	31	0.0096			0.0053
63	LH_Cont_Par_3	L_Angular gyrus	-45	-42	46	0.0071			0.0092
73	LH_Cont_Cing_2	L_Dorsal anterior cingulate gyrus	-3	4	30			0.0090	
94	LH_Default_PFC_12	L_Superior frontal gyrus (posterior segment)	-24	25	49			0.0283	
99	LH_Default_pCunPCC_4	L_Precuneous/Posterior Cingulate Cortex	-6	-54	42		0.0253		
117	RH_SomMot_2	R_Superior temporal gyrus	64	-23	8	0.0215			
122	RH_SomMot_7	R_Postcentral gyrus	58	-5	31		0.0237		
138	RH_DorsAttn_Post_4	R_Angular gyrus	46	-38	49			0.0055	
139	RH_DorsAttn_Post_5	R_Superior parietal gyrus	41	-31	46		0.0111		
187	RH_Default_Temp_3	R_Superior temporal gyrus	55	-6	-10			0.0174	
188	RH_Default_Temp_4	R_Middle temporal gyrus	63	-27	-6			0.0103	
200	RH_Default_pCunPCC_3	R_Precuneous/Posterior Cingulate Cortex	6	-58	44		0.0125		

Abbreviations: *MNI* Montreal Neurological Institute space; *LH* left hemisphere; *RH* right hemisphere; *SomMot_1*, *SomMot_2*, *SomMot_7*, *SomMot_11*, *SomMot_16*, first, second, seventh, eleventh, and sixteenth segment of the Somatomotor Network parcel; *DorsAttn_Post_4*, *DorsAttn_Post_5*, fourth and fifth segment of the Posterior Dorsal Attentional Network parcel; *SalVentAttn_ParOper_3*, third segment of the Parietal Operculum Salience/Ventral Attention Network parcel; *SalVentAttn_PFC1_1*, first segment of the Lateral Prefrontal Cortex Salience/Ventral Attention Network parcel; *Cont_Par_3*, third segment of the Parietal Control Network parcel; *Cont_Cing_2*, second segment of the Cingulate Control Network parcel; *Default_Temp_3*, *Default_Temp_4*, third and fourth segment of the Temporal Default Network parcel; *Default_PFC_12*, twelfth segment of the Prefrontal Cortex Default Network parcel; *Default_pCunPCC_3*, *Default_pCunPCC_4*, third and fourth segment of the Precuneus Posterior Cingulate Cortex Default Network parcel.

Note: Labels from the Yeo and Schaefer Atlas, available from:

https://github.com/ThomasYeoLab/CBIG/blob/master/stable_projects/brain_parcellation/Schaefer2018_LocalGlobal/Parcellations/MNI/Centroid_coordinates/Schaefer2018_200P_arcel_7Networks_order_FSLMNI152_1mm.Centroid_RAS.csv.

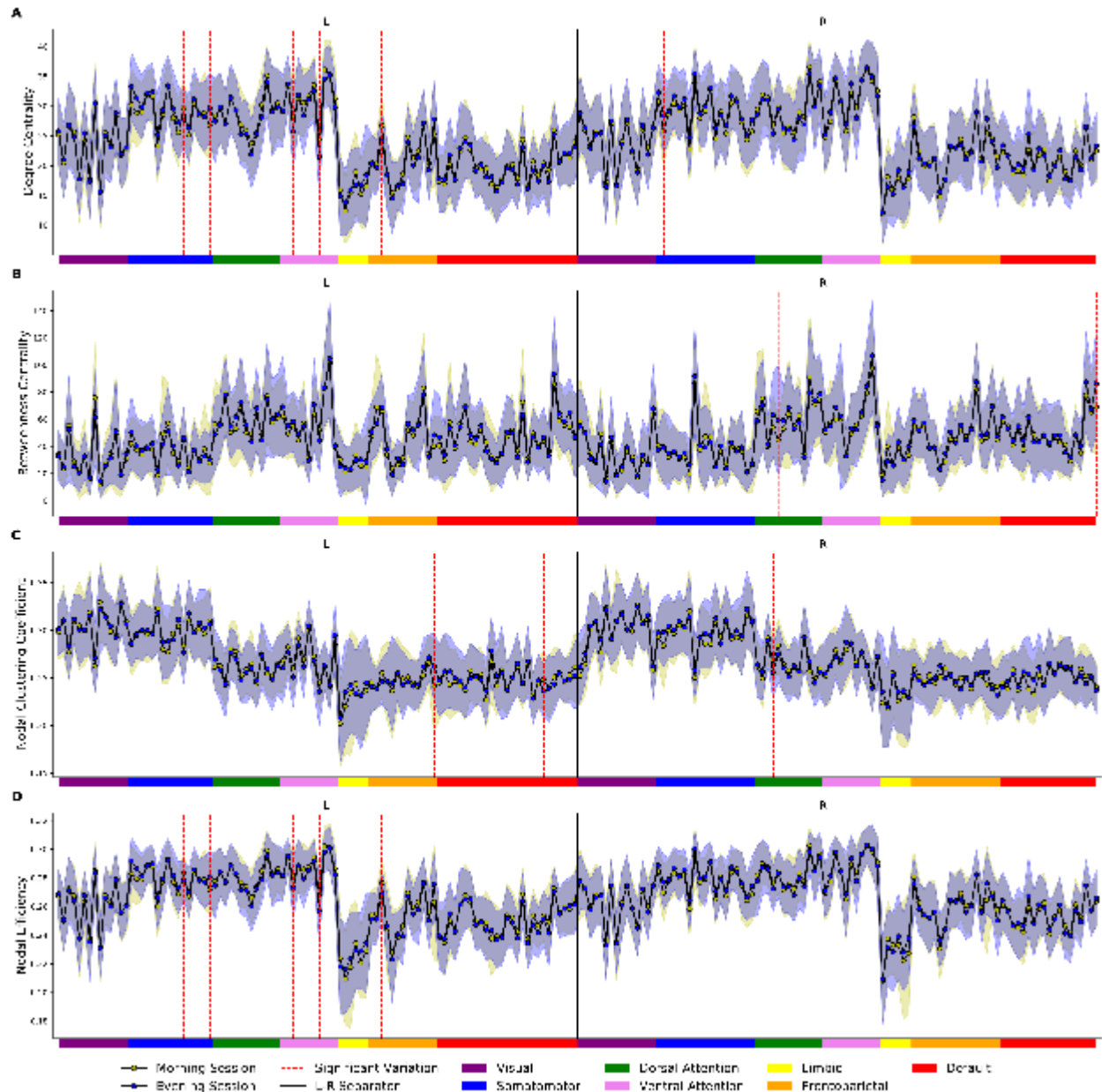


Figure 5. Area under the curve in the morning and evening sessions for degree centrality (A), betweenness centrality (B), clustering coefficient (C), and nodal efficiency (D) of all 200 ROIs. Each node (either in the left or right hemisphere) is labeled by a color matched to Schaefer/Yeo 7 network parcellation. Significant diurnal changes are represented by dashed red lines.

3.3. Hub analysis

In this subsection, using a pre-determined modular classification, which includes the visual, somatomotor, dorsal attention, ventral attention, limbic, frontoparietal, and default mode network (Yeo et al., 2011), we identified network hubs along with their types (i.e., connector or provincial) in both morning and evening sessions (**Table 4**). The results are based on the mean connectivity matrix (across all participants for each corresponding session), and for simplicity in visualizing them later, we chose network density of 0.05. As presented in **Table 4**, the identified hubs are

almost overlapping in the morning and evening sessions, except for minor changes in areas such as right SomMot_3 (posterior insula), right Post_5 (superior parietal gyrus), right PrCv_1 (precentral gyrus), and left pCun_1 (cuneus). We found that approximately 25% of somatomotor network nodes play a hub role in both morning and evening sessions, making this module the densest part of the brain during resting state. Notably, somatomotor hubs are either provincial (i.e., within modular connections) or connector (i.e., between modular connections), while hubs in the ventral attention network are connector and hubs in the visual network are provincial.

To visualize the results, connectograms of both sessions are illustrated in **Figure 6** using Circos software (Krzyszowski et al., 2009). Parcellated elements on the outermost circle indicate the 200 Schaefer/Yeo brain areas marked with a unique RGB code and belong to one of the predefined modules in each hemisphere. This outer circle circumscribes five inner circular heatmaps created to represent the values of five distinct centrality measures. The range for each of these measures is from the minimum to maximum assumed value. Toward the center, these measures are degree centrality, participation coefficient, K-core centrality, eigenvector centrality, and PageRank. The values of all measures, as well as the functional connections in each of the connectograms, are derived from the average of all individuals in the corresponding session. The red and black curves show the functional connections between and within modules, respectively. An unambiguous abbreviation scheme was created to label each parcellation, as summarized in Appendix Table A1.

Table 4. Identifying hubs in each brain network for both sessions (at a sparsity of 0.05).

Networks	L/R	Nodes	Session	Hubs (P, C)	Hub Regions ^(Type)
Visual	L	14	M	3 (3, 0)	Vis_1 ^(P) , Vis_13 ^(P) , Vis_14 ^(P)
			E	3 (3, 0)	Vis_1 ^(P) , Vis_13 ^(P) , Vis_14 ^(P)
	R	15	M	3 (3, 0)	Vis_3 ^(P) , Vis_4 ^(P) , Vis_12 ^(P)
			E	3 (3, 0)	Vis_3 ^(P) , Vis_4 ^(P) , Vis_12 ^(P)
Somatomotor	L	16	M	4 (2, 2)	SomMot_4 ^(C) , SomMot_5 ^(C) , SomMot_8 ^(P) , SomMot_13 ^(P)
			E	4 (2, 2)	SomMot_4 ^(C) , SomMot_5 ^(C) , SomMot_8 ^(P) , SomMot_13 ^(C)
	R	19	M	5 (3, 2)	SomMot_5 ^(C) , SomMot_6 ^(C) , SomMot_11 ^(P) , SomMot_15 ^(P) , SomMot_16 ^(P)
			E	6 (4, 2)	SomMot_3^(P) , SomMot_5 ^(C) , SomMot_6 ^(C) , SomMot_11 ^(P) , SomMot_15 ^(P) , SomMot_16 ^(P)
Dorsal Attention	L	13	M	0 (0, 0)	—
			E	0 (0, 0)	—
	R	13	M	2 (0, 2)	Post_5^(C), PrCv_1^(C)
			E	0 (0, 0)	—
Ventral Attention	L	11	M	5 (0, 5)	ParOper_2 ^(C) , FrOper_1 ^(C) , FrOper_3 ^(C) , FrOper_4 ^(C) , Med_1 ^(C)
			E	5 (0, 5)	ParOper_2 ^(C) , FrOper_1 ^(C) , FrOper_3 ^(C) , FrOper_4 ^(C) , Med_1 ^(C)
	R	11	M	4 (0, 4)	TempOccPar_3 ^(C) , FrOper_2 ^(C) , FrOper_4 ^(C) , Med_1 ^(C)
			E	4 (0, 4)	TempOccPar_3 ^(C) , FrOper_2 ^(C) , FrOper_4 ^(C) , Med_1 ^(C)
Limbic	L	6	M	0 (0, 0)	—
			E	0 (0, 0)	—
	R	6	M	0 (0, 0)	—
			E	0 (0, 0)	—

Frontoparietal	L	13	M	0 (0, 0)	—
			E	1 (0, 1)	pCun_1 ^(C)
	R	17	M	1 (0, 1)	pCun_1 ^(C)
			E	1 (0, 1)	pCun_1 ^(C)
Default Mode	L	27	M	0 (1, 0)	pCunPCC_2 ^(P)
			E	0 (1, 0)	
	R	19	M	0 (0, 1)	pCunPCC_1 ^(C)
			E	0 (0, 1)	

Abbreviations: *L/R* left or right hemisphere; *M* morning; *E* evening session; *P* provincial; *C* connector.

Note: Regions information is provided in the Appendix Table A1.

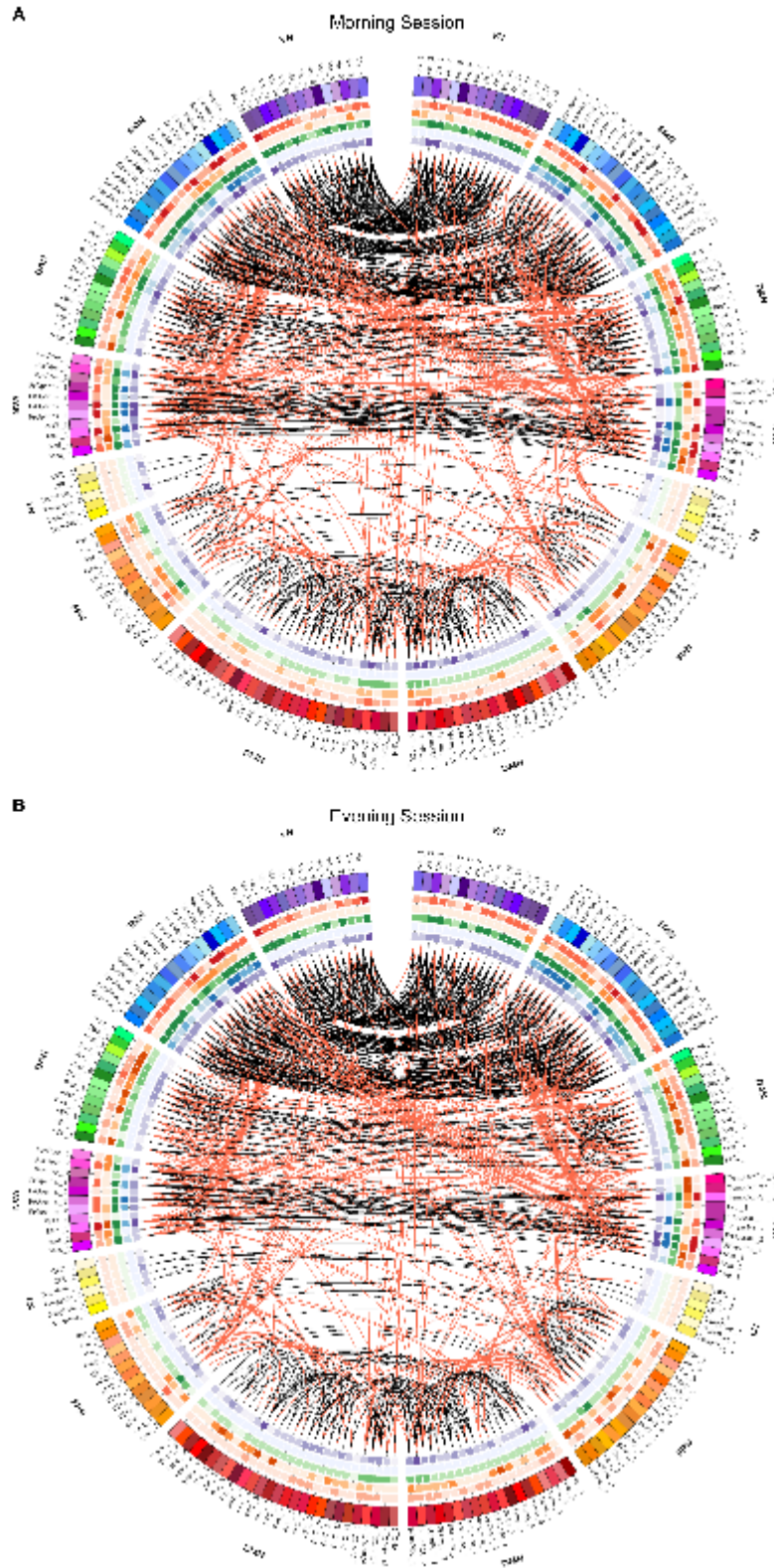


Figure 6. The mean connectogram across all participants in both morning (A) vs. evening (B) conditions at the thresholding value of 0.05. Abbreviations: *VN* visual network, *SMN* somatomotor network, *DAN* dorsal attention network, *VAN* ventral attention network, *LN* limbic network, *FPN* frontoparietal network, *DMN* default mode network.

3.4. Correlation analysis

A correlation analysis was performed to investigate whether global and nodal measures are significantly correlated with the variable of interest (e.g., ME scale, AM scale, ESS, or any other cognitive/behavioral variables) across subjects while controlling for the differences of the covariates of no interest (e.g., age, gender, and clinical variables). ME, AM, and ESS scores determine “person’s chronotype preference”, “how strong the preference is”, and “sleepiness during the day”, respectively. Overall, the number of significant associations was greater in the morning session rather than the evening session. From global perspective (**Table 5** and **Figure 7**), correlation analysis revealed significant negative associations between AM score and small-worldness and modularity in the morning session ($p < 0.05$, FDR corrected). We also found significant positive relations between ESS and average path length and assortativity in the morning session, as well as positive correlations between AM score and path length and assortativity in the evening session.

From a nodal perspective, we found significant correlations between degree centrality of various parts of the brain in both hemispheres and the subjective indicators (e.g., ME scale, AM scale, ESS), mostly across the morning scanning session (**Table 6** and **Figure 8**). In the morning session, there were significant negative correlations between: AM score and areas within the default network including left rostral anterior cingulate gyrus (Default_PFC_6), left precuneus (Default_PCC_2 and Default_PCC_4), right medial prefrontal cortex (Default_PFCm_4) and right posterior cingulate cortex (Default_PCC_2); ESS and left pole of superior temporal gyrus (Limbic_TempPole_3), right lateral fronto-orbital gyrus (Cont_PFCl_1) and right pole of middle temporal gyrus (Default_Temp_1); ME score and left postcentral gyrus (SomMot_4), left pole of superior temporal gyrus (Limbic_TempPole_4), as well as positive associations between: AM score and bilateral precentral gyrus (left DorsAttn_FEF_1 and right SomMot_11); ME score and bilateral insular (SalVentAttn_FrOper_2 and Cont_PFCv_1), left anterior cingulate gyrus (Default_PFC_8), and right precentral gyrus (DorsAttn_FEF_1).

During the evening session, there were significant positive associations between: AM score and left middle occipital gyrus (Vis_11), right fusiform gyrus (Vis_2) and right superior occipital gyrus (Vis_14), as well as negative correlations between: AM score and left precentral gyrus (DorsAttn_PrCv_1), bilateral lateral fronto-orbital gyrus (Limbic_OFC_1 and Limbic_OFC_2), and right middle temporal gyrus (Default_Temp_4). No significant correlation between ESS and ME scores and degree centrality of brain regions was found.

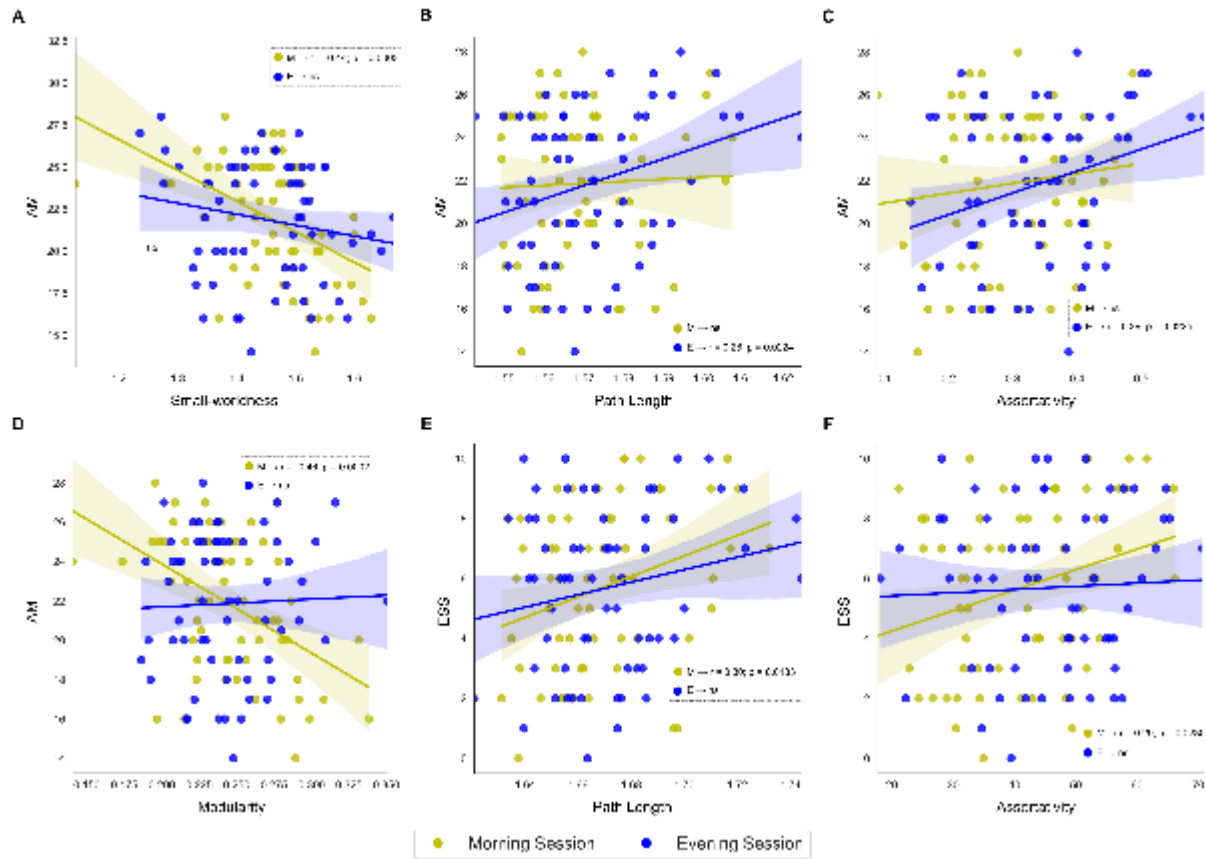


Figure 7. Significant associations between the global measures and questionnaire variables (AM, ESS and ME scores). AM and Small-worldness (A), AM and path length (B), AM and assortativity (C), AM and modularity (D), ESS and path length (E), and ESS and assortativity (D). Yellow and blue colors represent the scatterplots for morning and evening session, respectively. In each panel, one of the correlations related to the morning or evening session is statistically significant and the other is not-significant.

Table 5. Global analysis: significant correlations between global metrics and AM, ESS and ME scores (n = 62) for morning and evening sessions. The significance level is set at a $p < 0.05$ with non-parametric permutations.

	Correlation (adjusted p-value)					
	Morning session			Evening session		
	AM	ESS	ME	AM	ESS	ME
Small-worldness	-0.44 (0.0003)	—	—	—	—	—
Path Length	—	0.30 (0.0183)	—	0.28 (0.0224)	—	—
Modularity	-0.46 (0.0002)	—	—	—	—	—
Assortativity	—	0.29 (0.0230)	—	0.29 (0.0225)	—	—

Table 6. Nodal analysis: significant correlations between degree centrality and AM, ESS and ME scores (n = 62) for morning and evening sessions. The significance level is set at a $p < 0.05$ with non-parametric permutations.

ROI (Schaefer/Yeo Atlas)	Correlation (adjusted p-value)					
	Morning Session			Evening Session		
	AM	ESS	ME	AM	ESS	ME
Left Hemisphere	11 Vis_11				0.30 (0.0189)	
	18 SomMot_4			-0.37 (0.0029)		
	41 DorsAttn_FEF_1	0.38 (0.0023)				
	43 DorsAttn_PrCv_1				-0.33 (0.0091)	
	48 SalVentAttn_FrOper_2			0.37 (0.0024)		
	55 Limbic_OFC_1				-0.32 (0.0149)	
	59 Limbic_TempPole_3		-0.42 (0.0007)			
	60 Limbic_TempPole_4			-0.33 (0.0076)		
	88 Default_PFC_6	-0.32 (0.0113)				
	90 Default_PFC_8			0.30 (0.0200)		
97 Default_PCC_2	-0.39 (0.0015)					
99 Default_PCC_4	-0.32 (0.0093)					
Right Hemisphere	102 Vis_2				0.30 (0.0191)	
	114 Vis_14				0.31 (0.0159)	
	126 SomMot_11	0.30 (0.0172)				
	145 DorsAttn_FEF_1			0.33 (0.0080)		
	160 Limbic_OFC_2				-0.32 (0.0116)	
	169 Cont_PFCv_1			0.31 (0.0134)		
	170 Cont_PFCl_1		-0.31 (0.0153)			
	185 Default_Temp_1		-0.30 (0.0177)			
	188 Default_Temp_4				-0.31 (0.0128)	
	194 Default_PFCm_4	-0.37 (0.0032)				
199 Default_PCC_2	-0.29 (0.0195)					

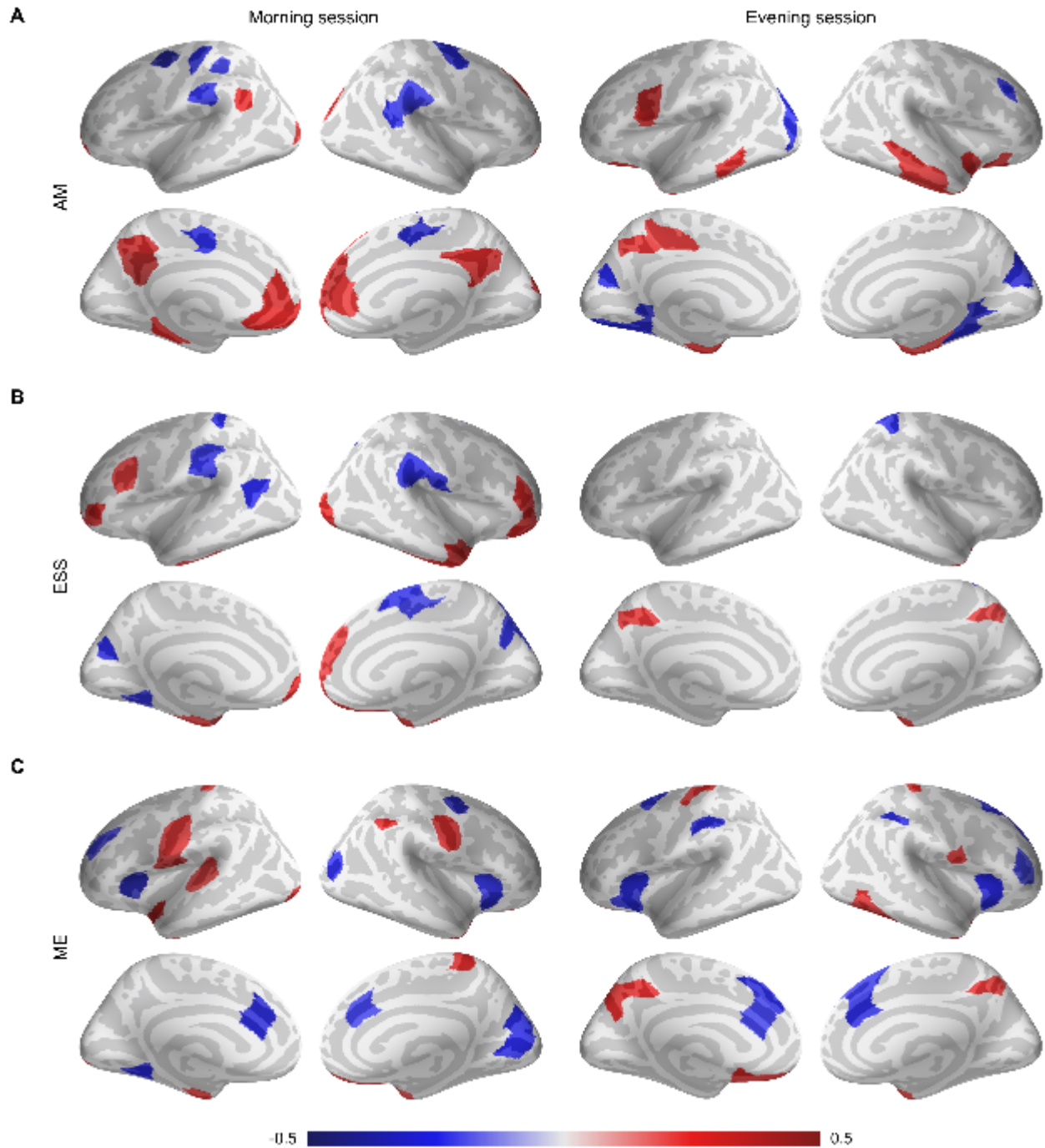


Figure 8. Correlation analysis between nodal centrality of brain regions and questionnaire variables AM (A), ESS (B), and ME (C). Nodes are colored according to their correlation magnitude.

4. Discussion

In this study, we used rs-fMRI and graph theory to examine diurnal fluctuation of whole-brain connectivity architectures across 62 healthy and young subjects, taking into account their chronotypes. The results of the study revealed meaningful information about the topological variations of the brain network during the day, as well as the associations of graph theoretical

metrics with the variables of interest (e.g., ME, AM, and ESS scores), which are as follows: (1) among the global measures, there was a significant increase in small-worldness, modularity, assortativity, and network synchronization in the evening session compared to the morning session ($p < 0.05$, FDR corrected), however, there was no compelling evidence of changes in any of the global metrics in terms of chronotype (i.e., between morning- and evening-type participants); (2) local graph measures varied (during the day) predominantly across the somatomotor, attention, and default mode network ($p < 0.05$, FDR corrected), however, local metrics were mainly consistent with chronotype changes ($p > 0.05$); (3) analysis of the hubs demonstrated that the somatomotor network was the densest area of the brain (at both sessions but more during the evening) with both provincial and connector types, while hubs in the ventral attention network and visual network were primarily connector and provincial, respectively; (4) correlation analysis revealed significant associations between the variables derived from the questionnaires (such as ME, AM, and ESS) and the nodal characteristics of a number of brain regions in both sessions, most of which were related to the morning session.

4.1. Diurnal variations in global properties

A small-world network is an intermediary between random and regular networks, consisting a large number of short-range connections alongside a few long-range shortcuts (Watts and Strogatz, 1998). In the real system, there are other ways to define it, e.g., by considering the physical length of connections, all of which mathematically believe that small-world networks share a relative high transitivity and small mean geodesic (i.e., shortest-path) distance between nodes. This property makes them superior to other networks in terms of functional segregation (local specialization) and integration (global information flow), respectively (Bassett and Bullmore, 2006; Rubinov and Sporns, 2010). In our analysis of rs-fMRI data, we found high values of small-worldness for both scanning sessions ($\sigma \geq 1$ generally represents an efficient network), albeit with significant superiority in the evening session at sparse networks compared to the morning session, which reflects a more efficient functional topology in the brain network. Also, as another segregation metric, we found higher modularity in the evening session compared to the morning session at lower sparsity, reflecting a better division of the brain network into specialized communities. In another study, Anderson et al. (2016) explored how TOD affects functional brain networks in older healthy adults during rest and the performance of task. They found no topological changes during the resting-state, and a decrease in small-worldness and modularity in the afternoon (3:00 pm) compared to the morning (8:00 am), during the performance of a 1-back task.

More specifically, the hypothalamic suprachiasmatic nucleus (SCN) network, the control center for the body's "biological clock", is thought to be scale-free (Barabási and Albert, 1999; Hafner et al., 2012) and to possess small-world characteristics (Vasalou et al., 2009). In this regard, various studies have reported that more small-worldness of the SCN leads to more precise circadian fluctuations, a larger amplitude, higher synchrony and shifts more rapidly after the emergence of a new light/dark cycle compared to purely random or regular networks (Bodenstein et al., 2012; Gu et al., 2016; Hafner et al., 2012; Šimonka et al., 2015; Vasalou et al., 2009; Webb et al., 2012).

Furthermore, our findings revealed an increase in network assortativity over the course of the day, which overlaps with our previous results (Farahani et al., 2019). Increased assortativity is

associated with a higher tendency for a node to link to other nodes with the same or similar degree (Newman, 2003; Foster et al., 2010), thus increasing the likelihood of a nearby hub supporting the faulty node. Finally, our results of network synchronization — a measure for assessing how well all nodes fluctuate in the same wave pattern — were not consistent with findings from Barahona and Pecora (2002), who presented that in networks of low redundancy, the small-world attitude results in more efficient synchrony than standard deterministic graphs, random graphs, and ideal constructive schemes. In fact, we found that in both the morning and evening sessions, as we move from low to high sparsity, small-worldness decreases, while synchronization increases. Notably, the network synchronization was significantly higher during the evening scanning session as compared to the morning. Overall, the findings of all global measures (i.e., small-worldness, modularity, assortativity, and synchronization) indicate that brain network organization varied throughout the day, which could be associated with increased brain function from morning to evening.

4.2. Nodal changes over the course of the day

To identify the nodal effects of TOD on the brain, a number of features, including degree centrality, betweenness centrality, clustering coefficient, and nodal efficiency, were extracted from each of the 200 ROIs. Accordingly, the somatomotor network (e.g., the bilateral superior temporal, parietal, and postcentral gyri), attention network (e.g., left supramarginal, left middle frontal, right angular, and right superior parietal), as well as default mode network (e.g., the bilateral posterior cingulate cortex/precuneus and angular gyrus) experienced the most topological variations among brain networks during the day. The study of hubs in these networks also demonstrated that they host several densely connected nodes, which strongly affect the brain functional integration and segregation.

Our resting-state findings showed that the within modular connectivity of the somatomotor network and its interaction with other parts of the brain (particularly, the ventral attention network) in both morning and evening sessions were relatively higher than other brain networks. Connectivity and hub analyses showed that the somatomotor network is the most densely-connected system in the brain predominantly during the evening session. We also found significantly increased FC in the bilateral postcentral, superior temporal, and superior parietal gyri as the waking time increases. Consistent with our results, such changes in the neural response across TOD have been previously reported in other rs-fMRI studies (Anderson et al., 2014; Fafrowicz et al., 2019; Jiang et al., 2016; Maire et al., 2018), as well as magnetoencephalography (MEG) studies to evaluate oscillatory activity at rest and during a finger-tapping task (Wilson et al., 2014). However, through a morphometric approach, conflicting results were found by Trefler et al. (2016) who discovered apparent decrease of cortical thickness as a function of TOD across the lateral surfaces of the left frontal, temporal, and parietal lobes. Together, our findings provide insight into how coordinated activity in sensorimotor networks vary over the course of the day. The increase of FC in somatomotor regions during the day indicate that neural synchronization is enhanced in these areas as a result of compensatory efforts to combat exhaustiveness, sleepiness, and absentmindedness after a day experience.

Ventral and dorsal attention networks regions are reported to be involved in stimulus-driven and goal-directed attention, respectively (Vossel et al., 2013). Connectivity and hub analyses showed that the ventral attention system is the second densely-connected network after the somatomotor areas mostly during the morning session with a focus on the frontal operculum insula and dorsal anterior cingulate gyrus. We also found a decreased FC throughout the course of the day within ventral areas such as the left supramarginal gyrus and left middle frontal gyrus (dorsal prefrontal cortex), in agreement with previous studies (Anderson et al., 2016; Jiang et al., 2016; Vandewalle et al., 2009). Also, changes were also observed in the right dorsal attention areas such as angular and superior parietal gyri. Drummond and Brown (2001) reported that total sleep deprivation was associated with increased activation in the prefrontal cortex and parietal lobes in learning and attention tasks, implying a compensatory mechanism for fighting against sleepiness. Overall, our results showed that due to increased sleepiness or fatigue during the day, the brain could not adapt to fulfill the demand for the attention and alertness even at early evening hours.

The DMN consists of a set of functionally connected and specialized neural units that contribute to many cognitive functions, including self-referential processing, autobiographical memory, and memory consolidation (Andrews-Hanna et al., 2007; Mayer et al., 2010; Raichle et al., 2001). Our study showed that the DMN is involved in relatively high neural activity at resting state during both sessions, particularly in the posterior cingulate cortex/precuneus which we detected it as a hub (higher in the evening than in the morning), and it plays a key role in the mediation of intrinsic activity through DMN (Fransson and Marrelec, 2008). Some areas within the DMN were found to be prone to variations in their connectivity profiles across daytime, such as the bilateral posterior cingulate cortex/precuneus, angular gyrus, superior temporal gyrus, and left superior frontal gyrus, a finding consistent with previous rs-fMRI studies (Facer-Childs et al., 2019b; Fransson, 2005; Jiang et al., 2016; Ku et al., 2018; Orban et al., 2020; Raichle et al., 2001; Shannon et al., 2013). Also, Blautzik et al. (2013) and Hodkinson et al. (2014) reported a rhythmic FC pattern of DMN during the day with its peak in the morning and declining trend in the afternoon. Diurnal changes in these areas indicate the functional coordination of the spatially disparate gyri (Jiang et al., 2016). Evidence has also pointed to a decrease in the default mode FC in sleep restriction as compared with the fully rested wakefulness (De Havas et al., 2012; Farahani et al., 2019). Considering these findings, total DMN neural activity decreased during the day, however, the FC increased in the hub regions such as posterior cingulate cortex/precuneus, which indicates the redoubled and regulatory efforts of these areas to balance of neuronal interconnections (coupling or decoupling) within DMN subregions and adapt the network under continued wakeful condition across the course of a day.

4.3. Limitations and future directions

There are certain limitations associated with this study that should be considered in future research. First, brain nodes were derived from the cortical Schaefer/Yeo atlas (200-parcel/7-network parcellation; Schaefer et al., 2018). Schaefer's parcellations are available at multiple resolution (100 parcels to 1000 parcels), thus further investigation appraising network topology using finer parcellation schemes are warranted. Also, since the Schaefer atlas only considers cortical areas, whole-brain studies could be carried out by adding subcortical regions with the help of other atlases or segmentation algorithms. This issue should be investigated in more detail in future studies.

A second limitation concerns the measures used to compare the group-representative functional brain networks to one another. These measures tend to be correlated with one another — for example, a brain network with high efficiency necessarily must have shorter path length (Betzel et al., 2018). Thus, if one finds significant differences in one measure, it will probably be found in others. Therefore, given that we have chosen several correlated measures in this study, our analyses could be extended in future work to identify which of these measures is driving the others and how an exhaustive set of metrics can be designed to neurobiologically fit the study specification. Another issue about network measures is that global statistics are often non-specific (i.e., not especially informative). For example, the phrase “the patient group has lower efficiency than control” may not be clear to a neurosurgeon, so future work should be directed to investigate better interpretations of such metrics.

Yet another limitation concerns the applicability of small-world property. In real systems, early definitions of small-worldness, initiated by Watts and Strogatz (1998a), are ineffective for reasons such as confusing regular networks instead of small-world structure, neglecting the weight and physical length of connections, and lack of attention to the network density. Most of them present the network on the border of a circle, but real systems aren’t embedded that way. Luckily, there are many different ways for a network to be small-world besides starting from a regular network and adding random links that reduce path length and researchers addressed the mentioned constraints by introducing several practical metrics (Bolaños et al., 2013; Muldoon et al., 2016; Rubinov and Sporns, 2010; Telesford et al., 2011). Applying these modified metrics in future work brings the study of small-world brain closer to reality.

Several theory-driven techniques have recently emerged to highlight the importance of machine learning, algorithmic optimization, and parallel computing in functional neuroimaging (Cohen et al., 2017; Douglas et al. 2013). For example, various algorithms called graph neural networks, of which Graph Convolutional Networks (GCN) being one of them, have been proposed that show how graph theory can be used as features to train deep learning models (Kipf and Welling, 2016; Wu et al., 2020) and discover neurological biomarkers using fMRI data (Li et al., 2020). As another example, a growing trend has developed in a family of algorithms called hyperalignment (or functional alignment) for projecting individuals’ data into a common space based on how voxels respond to stimuli (Guntupalli et al., 2016; Haxby et al., 2011) or are connected to other voxels (Guntupalli et al., 2018; Haxby et al., 2020). The combined use of these techniques with network neuroscience will open a new generation of studies to transform knowledge of neural representations in complex brain networks.

5. Conclusion

Here, we present evidence for topological changes in functional brain network over the course of the day, i.e., in the morning as compared to the evening (1 and 10 hours after the wake-up time, respectively), using rs-fMRI data combined with graph theoretical analysis. Compared to the morning session, we found a more efficient functional topology in the evening session based on the global examination. Local properties differed prominently across the somatomotor, ventral attention, and default mode networks. In this way, we also considered inter-individual differences in diurnal preferences (chronotypes; early larks or night owls) in addition to the effect of TOD,

however, we did not find any significant difference between the chronotypes. In summary, our findings can reveal insight into diurnal variations in resting brain network and emphasize the role of TOD when designing neuroimaging experiments.

References

- Anderson, J. A. E., Campbell, K. L., Amer, T., Grady, C. L., and Hasher, L. (2014). Timing is everything: Age differences in the cognitive control network are modulated by time of day. *Psychol. Aging* 29, 648–657. doi:10.1037/a0037243.
- Anderson, J. A. E., Sarraf, S., Amer, T., Bellana, B., Man, V., Campbell, K. L., et al. (2016). Task-linked Diurnal Brain Network Reorganization in Older Adults: A Graph Theoretical Approach. *J. Cogn. Neurosci.* 29, 560–572. doi:10.1162/jocn_a_01060.
- Andrews-Hanna, J. R., Snyder, A. Z., Vincent, J. L., Lustig, C., Head, D., Raichle, M. E., et al. (2007). Disruption of large-scale brain systems in advanced aging. *Neuron* 56, 924–935. doi:10.1016/j.neuron.2007.10.038.
- Aoyama, S., and Shibata, S. (2017). The Role of Circadian Rhythms in Muscular and Osseous Physiology and Their Regulation by Nutrition and Exercise. *Front. Neurosci.* 11, 63. doi:10.3389/fnins.2017.00063.
- Bailey, S. L., and Heitkemper, M. M. (2001). Circadian rhythmicity of cortisol and body temperature: morningness-eveningness effects. *Chronobiol. Int.* 18, 249–261. doi:10.1081/CBI-100103189.
- Barabási, A.-L., and Albert, R. (1999). Emergence of Scaling in Random Networks. *Science* (80-.). 286, 509 LP – 512. doi:10.1126/science.286.5439.509.
- Barahona, M., and Pecora, L. M. (2002). Synchronization in small-world systems. *Phys. Rev. Lett.* 89, 54101. doi:10.1103/PhysRevLett.89.054101.
- Bassett, D. S., and Bullmore, E. (2006). Small-world brain networks. *Neuroscientist* 12, 512–523. doi:10.1177/1073858406293182.
- Behzadi, Y., Restom, K., Liau, J., and Liu, T. T. (2007). A component based noise correction method (CompCor) for BOLD and perfusion based fMRI. *Neuroimage* 37, 90–101. doi:https://doi.org/10.1016/j.neuroimage.2007.04.042.
- Betz, R. F., Griffa, A., Hagmann, P., and Mišić, B. (2018). Distance-dependent consensus thresholds for generating group-representative structural brain networks. *Netw. Neurosci.* 3, 475–496. doi:10.1162/netn_a_00075.
- Blautzik, J., Vetter, C., Peres, I., Gutyrchik, E., Keeser, D., Berman, A., et al. (2013). Classifying fMRI-derived resting-state connectivity patterns according to their daily rhythmicity. *Neuroimage* 71, 298–306. doi:https://doi.org/10.1016/j.neuroimage.2012.08.010.
- Bodenstein, C., Gosak, M., Schuster, S., Marhl, M., and Perc, M. (2012). Modeling the Seasonal Adaptation of Circadian Clocks by Changes in the Network Structure of the Suprachiasmatic Nucleus. *PLOS Comput. Biol.* 8, e1002697. Available at: https://doi.org/10.1371/journal.pcbi.1002697.

- Bolaños, M., Bernat, E. M., He, B., and Aviyente, S. (2013). A weighted small world network measure for assessing functional connectivity. *J. Neurosci. Methods* 212, 133–142. doi:10.1016/j.jneumeth.2012.10.004.
- Borbély, A. A. (1982). A two process model of sleep regulation. *Hum neurobiol* 1, 195–204. doi:10.1007/978-3-540-29678-2_6166.
- Cohen, J. D., Daw, N., Engelhardt, B., Hasson, U., Li, K., Niv, Y., et al. (2017). Computational approaches to fMRI analysis. *Nat. Neurosci.* 20, 304–313. doi:10.1038/nn.4499.
- Cordani, L., Tagliazucchi, E., Vetter, C., Hassemer, C., Roenneberg, T., Stehle, J. H., et al. (2018). Endogenous modulation of human visual cortex activity improves perception at twilight. *Nat. Commun.* 9, 1274. doi:10.1038/s41467-018-03660-8.
- De Havas, J. A., Parimal, S., Soon, C. S., and Chee, M. W. L. (2012). Sleep deprivation reduces default mode network connectivity and anti-correlation during rest and task performance. *Neuroimage* 59, 1745–1751. doi:https://doi.org/10.1016/j.neuroimage.2011.08.026.
- Dijk, D.-J., and Lockley, S. W. (2002). Invited Review: Integration of human sleep-wake regulation and circadian rhythmicity. *J. Appl. Physiol.* 92, 852–862. doi:10.1152/jappphysiol.00924.2001.
- Douglas, PK, Lau, E, Anderson, A, Kerr, W, Head, A, Wollner, M, Moyer, D, Durnhofer, M, Li, W, Bramen, J, Cohen, MS. (2013) Single Trial decoding of belief decision making from EEG and fMRI data using independent components features. *Frontiers in human neuroscience.* 7, 392.
- Drummond, S. P. A., and Brown, G. G. (2001). The Effects of Total Sleep Deprivation on Cerebral Responses to Cognitive Performance. *Neuropsychopharmacology* 25, S68–S73. doi:https://doi.org/10.1016/S0893-133X(01)00325-6.
- Edwards, B., Waterhouse, J., and Reilly, T. (2007). The Effects of Circadian Rhythmicity and Time-Awake on a Simple Motor Task. *Chronobiol. Int.* 24, 1109–1124. doi:10.1080/07420520701795316.
- Facer-Childs, E. R., Campos, B. M., Middleton, B., Skene, D. J., and Bagshaw, A. P. (2019a). Circadian phenotype impacts the brain’s resting-state functional connectivity, attentional performance, and sleepiness. *Sleep* 42. doi:10.1093/sleep/zsz033.
- Facer-Childs, E. R., Campos, B. M., Middleton, B., Skene, D. J., and Bagshaw, A. P. (2019b). Circadian phenotype impacts the brain’s resting-state functional connectivity, attentional performance, and sleepiness. *Sleep* 42, 1–12. doi:10.1093/sleep/zsz033.
- Fafrowicz, M., Bohaterewicz, B., Ceglarek, A., Cichocka, M., Lewandowska, K., Sikora-Wachowicz, B., et al. (2019). Beyond the Low Frequency Fluctuations: Morning and Evening Differences in Human Brain. *Front. Hum. Neurosci.* 13, 1–6. doi:10.3389/fnhum.2019.00288.
- Fafrowicz, M., Golonka, K., Marek, T., Mojsa-Kaja, J., Tucholska, K., Oginska, H., et al. (2009). Diurnal variability of human operator attention disengagement and chronotype: an fMRI-based case study. *Theor. Issues Ergon. Sci.* 10, 545–557. doi:10.1080/14639220902992001.

- Farahani, F. V., Fafrowicz, M., Karwowski, W., Douglas, P. K., Domagalik, A., Beldzik, E., et al. (2019). Effects of Chronic Sleep Restriction on the Brain Functional Network, as Revealed by Graph Theory. *Front. Neurosci.* 13, 1087. doi:10.3389/fnins.2019.01087.
- Fransson, P. (2005). Spontaneous low-frequency BOLD signal fluctuations: An fMRI investigation of the resting-state default mode of brain function hypothesis. *Hum. Brain Mapp.* 26, 15–29. doi:10.1002/hbm.20113.
- Fransson, P., and Marrelec, G. (2008). The precuneus/posterior cingulate cortex plays a pivotal role in the default mode network: Evidence from a partial correlation network analysis. *Neuroimage* 42, 1178–1184. doi:https://doi.org/10.1016/j.neuroimage.2008.05.059.
- Freeman, L. C. (1978). Centrality in Social Networks Conceptual Clarification. *Soc. Networks* 1, 215–239. doi:10.1016/0378-8733(78)90021-7.
- Gamboa, O. L., Tagliazucchi, E., Von Wegner, F., Jurcoane, A., Wahl, M., Laufs, H., et al. (2014). Working memory performance of early MS patients correlates inversely with modularity increases in resting state functional connectivity networks. *Neuroimage* 94, 385–395. doi:10.1016/j.neuroimage.2013.12.008.
- Gilestro, G. F., Tononi, G., and Cirelli, C. (2009). Widespread Changes in Synaptic Markers as a Function of Sleep and Wakefulness in Drosophila. *Science (80-.)*. 324, 109–112. doi:10.1126/science.1166673.
- Gorfine, T., Yeshurun, Y., and Zisapel, N. (2007). Nap and melatonin-induced changes in hippocampal activation and their role in verbal memory consolidation. *J. Pineal Res.* 43, 336–342. doi:10.1111/j.1600-079X.2007.00482.x.
- Gu, C., Liang, X., Yang, H., and Rohling, J. H. T. (2016). Heterogeneity induces rhythms of weakly coupled circadian neurons. *Sci. Rep.* 6, 21412. doi:10.1038/srep21412.
- Guimerà, R., and Nunes Amaral, L. A. (2005). Functional cartography of complex metabolic networks. *Nature* 433, 895. Available at: <https://doi.org/10.1038/nature03288>.
- Guntupalli, J. S., Feilong, M., and Haxby, J. V. (2018). A computational model of shared fine-scale structure in the human connectome. *PLOS Comput. Biol.* 14, e1006120. Available at: <https://doi.org/10.1371/journal.pcbi.1006120>.
- Guntupalli, J. S., Hanke, M., Halchenko, Y. O., Connolly, A. C., Ramadge, P. J., and Haxby, J. V. (2016). A Model of Representational Spaces in Human Cortex. *Cereb. Cortex* 26, 2919–2934. doi:10.1093/cercor/bhw068.
- Hafner, M., Koepl, H., and Gonze, D. (2012). Effect of Network Architecture on Synchronization and Entrainment Properties of the Circadian Oscillations in the Suprachiasmatic Nucleus. *PLOS Comput. Biol.* 8, e1002419. Available at: <https://doi.org/10.1371/journal.pcbi.1002419>.
- Hastings, M., O'Neill, J. S., and Maywood, E. S. (2007). Circadian clocks: regulators of endocrine and metabolic rhythms. *J. Endocrinol.* 195, 187–198. doi:10.1677/JOE-07-0378.
- Haxby, J. V., Guntupalli, J. S., Connolly, A. C., Halchenko, Y. O., Conroy, B. R., Gobbini, M. I., et al. (2011). A Common, High-Dimensional Model of the Representational Space in

- Human Ventral Temporal Cortex. *Neuron* 72, 404–416.
doi:<https://doi.org/10.1016/j.neuron.2011.08.026>.
- Haxby, J. V., Guntupalli, J. S., Nastase, S. A., and Feilong, M. (2020). Hyperalignment: Modeling shared information encoded in idiosyncratic cortical topographies. *Elife* 9, e56601. doi:[10.7554/eLife.56601](https://doi.org/10.7554/eLife.56601).
- Hodkinson, D. J., O'Daly, O., Zunszain, P. A., Pariante, C. M., Lazurenko, V., Zelaya, F. O., et al. (2014). Circadian and Homeostatic Modulation of Functional Connectivity and Regional Cerebral Blood Flow in Humans under Normal Entrained Conditions. *J. Cereb. Blood Flow Metab.* 34, 1493–1499. doi:[10.1038/jcbfm.2014.109](https://doi.org/10.1038/jcbfm.2014.109).
- Horne, J. A., Brass, C. G., and Petitt, A. N. (1980). Circadian performance differences between morning and evening 'types.' *Ergonomics* 23, 29–36. doi:[10.1080/00140138008924715](https://doi.org/10.1080/00140138008924715).
- Humphries, M. D., and Gurney, K. (2008). Network “small-world-ness”: A quantitative method for determining canonical network equivalence. *PLoS One* 3. doi:[10.1371/journal.pone.0002051](https://doi.org/10.1371/journal.pone.0002051).
- Jiang, C., Yi, L., Su, S., Shi, C., Long, X., Xie, G., et al. (2016). Diurnal Variations in Neural Activity of Healthy Human Brain Decoded with Resting-State Blood Oxygen Level Dependent fMRI. *Front. Hum. Neurosci.* 10, 634. doi:[10.3389/fnhum.2016.00634](https://doi.org/10.3389/fnhum.2016.00634).
- Johns, M. W. (1991). A new method for measuring daytime sleepiness: the Epworth sleepiness scale. *Sleep* 14, 540–545. doi:[10.1093/sleep/14.6.540](https://doi.org/10.1093/sleep/14.6.540).
- Kerkhof, G. A., and Dongen, H. P. A. Van (1996). Morning-type and evening-type individuals differ in the phase position of their endogenous circadian oscillator. *Neurosci. Lett.* 218, 153–156. doi:[https://doi.org/10.1016/S0304-3940\(96\)13140-2](https://doi.org/10.1016/S0304-3940(96)13140-2).
- Kipf, T. N., and Welling, M. (2016). Semi-Supervised Classification with Graph Convolutional Networks. *arXiv e-prints*, arXiv:1609.02907.
- Krzywinski, M., Schein, J., Birol, I., Connors, J., Gascoyne, R., Horsman, D., et al. (2009). Circos: an information aesthetic for comparative genomics. *Genome Res.* 19, 1639–1645.
- Ku, J., Lee, Y. S., Chang, H. W., Earley, C. J., Allen, R. P., and Cho, Y. W. (2018). Diurnal variation of default mode network in patients with restless legs syndrome. *Sleep Med.* 41, 1–8. doi:<https://doi.org/10.1016/j.sleep.2017.09.031>.
- Kuhn, M., Wolf, E., Maier, J. G., Mainberger, F., Feige, B., Schmid, H., et al. (2016). Sleep recalibrates homeostatic and associative synaptic plasticity in the human cortex. *Nat. Commun.* 7, 12455. doi:[10.1038/ncomms12455](https://doi.org/10.1038/ncomms12455).
- Latora, V., and Marchiori, M. (2001). Efficient behavior of small-world networks. *Phys. Rev. Lett.* 87, 198701-1-198701-4. doi:[10.1103/PhysRevLett.87.198701](https://doi.org/10.1103/PhysRevLett.87.198701).
- Li, X., Zhou, Y., Gao, S., Dvornek, N., Zhang, M., Zhuang, J., et al. (2020). BrainGNN: Interpretable Brain Graph Neural Network for fMRI Analysis. *bioRxiv*. doi:[10.1101/2020.05.16.100057](https://doi.org/10.1101/2020.05.16.100057).
- Liu, T. T., Nalci, A., and Falahpour, M. (2017). The global signal in fMRI: Nuisance or

- Information? *Neuroimage* 150, 213–229.
doi:<https://doi.org/10.1016/j.neuroimage.2017.02.036>.
- Maire, M., Reichert, C. F., Gabel, V., Viola, A. U., Phillips, C., Berthomier, C., et al. (2018). Human brain patterns underlying vigilant attention: impact of sleep debt, circadian phase and attentional engagement. *Sci. Rep.* 8, 970. doi:10.1038/s41598-017-17022-9.
- Mayer, J. S., Roebroek, A., Maurer, K., and Linden, D. E. J. (2010). Specialization in the default mode: Task-induced brain deactivations dissociate between visual working memory and attention. *Hum. Brain Mapp.* 31, 126–139. doi:10.1002/hbm.20850.
- Muldoon, S. F., Bridgeford, E. W., and Bassett, D. S. (2016). Small-world propensity and weighted brain networks. *Sci. Rep.* 6, 1–13. doi:10.1038/srep22057.
- Newman, M. E. J. (2002). Assortative mixing in networks. *Phys. Rev. Lett.* 89, 208701.
- Newman, M. E. J. (2004). Fast algorithm for detecting community structure in networks. *Phys. Rev. E* 69, 66133.
- Nichols, T. E., and Holmes, A. P. (2002). Nonparametric permutation tests for functional neuroimaging: A primer with examples. *Hum. Brain Mapp.* 15, 1–25.
doi:<https://doi.org/10.1002/hbm.1058>.
- Norbury, R. (2020). Diurnal Preference and Grey Matter Volume in a Large Population of Older Adults: Data from the UK Biobank. *J. Circadian Rhythms* 18.
- Oginska, H., Mojsa-Kaja, J., and Mairesse, O. (2017). Chronotype description: In search of a solid subjective amplitude scale. *Chronobiol. Int.* 34, 1388–1400.
doi:10.1080/07420528.2017.1372469.
- Oldfield, R. C. (1971). The assessment and analysis of handedness: The Edinburgh inventory. *Neuropsychologia* 9, 97–113. doi:[https://doi.org/10.1016/0028-3932\(71\)90067-4](https://doi.org/10.1016/0028-3932(71)90067-4).
- Orban, C., Kong, R., Li, J., Chee, M. W. L., and Yeo, B. T. T. (2020). Time of day is associated with paradoxical reductions in global signal fluctuation and functional connectivity. *PLOS Biol.* 18, e3000602. Available at: <https://doi.org/10.1371/journal.pbio.3000602>.
- Peres, I., Vetter, C., Blautzik, J., Reiser, M., Pöppel, E., Meindl, T., et al. (2011). Chronotype Predicts Activity Patterns in the Neural Underpinnings of the Motor System During the Day. *Chronobiol. Int.* 28, 883–889. doi:10.3109/07420528.2011.619084.
- Power, J. D., Cohen, A. L., Nelson, S. M., Wig, G. S., Barnes, K. A., Church, J. A., et al. (2011). Functional Network Organization of the Human Brain. *Neuron* 72, 665–678.
doi:10.1016/j.neuron.2011.09.006.
- Raichle, M. E., MacLeod, A. M., Snyder, A. Z., Powers, W. J., Gusnard, D. A., and Shulman, G. L. (2001). A default mode of brain function. *Proc. Natl. Acad. Sci.* 98, 676 LP – 682.
doi:10.1073/pnas.98.2.676.
- Ramírez, C., Talamantes, J., García, A., Morales, M., Valdez, P., and Menna-Barreto, L. (2006). Circadian rhythms in phonological and visuospatial storage components of working memory. *Biol. Rhythm Res.* 37, 433–441. doi:10.1080/09291010600870404.

- Refinetti, R., and Menaker, M. (1992). The circadian rhythm of body temperature. *Physiol. Behav.* 51, 613–637. doi:[https://doi.org/10.1016/0031-9384\(92\)90188-8](https://doi.org/10.1016/0031-9384(92)90188-8).
- Roenneberg, T., Wirz-Justice, A., and Mellow, M. (2003). Life between Clocks: Daily Temporal Patterns of Human Chronotypes. *J. Biol. Rhythms* 18, 80–90. doi:10.1177/0748730402239679.
- Rubinov, M., and Sporns, O. (2010). Complex network measures of brain connectivity: Uses and interpretations. *Neuroimage* 52, 1059–1069. doi:10.1016/j.neuroimage.2009.10.003.
- Schaefer, A., Kong, R., Gordon, E. M., Laumann, T. O., Zuo, X.-N., Holmes, A. J., et al. (2018). Local-Global Parcellation of the Human Cerebral Cortex from Intrinsic Functional Connectivity MRI. *Cereb. Cortex* 28, 3095–3114. doi:10.1093/cercor/bhx179.
- Schmidt, C., Collette, F., Cajochen, C., and Peigneux, P. (2007). A time to think: Circadian rhythms in human cognition. *Cogn. Neuropsychol.* 24, 755–789. doi:10.1080/02643290701754158.
- Schmidt, C., Collette, F., Leclercq, Y., Sterpenich, V., Vandewalle, G., Berthomier, P., et al. (2009). Homeostatic sleep pressure and responses to sustained attention in the suprachiasmatic area. *Science (80-.)*. 324, 516–519. doi:10.1126/science.1167337.
- Schmidt, C., Collette, F., Reichert, C. F., Maire, M., Vandewalle, G., Peigneux, P., et al. (2015). Pushing the Limits: Chronotype and Time of Day Modulate Working Memory-Dependent Cerebral Activity. *Front. Neurol.* 6, 199. doi:10.3389/fneur.2015.00199.
- Schmidt, C., Peigneux, P., Leclercq, Y., Sterpenich, V., Vandewalle, G., Phillips, C., et al. (2012). Circadian preference modulates the neural substrate of conflict processing across the day. *PLoS One* 7, e29658. doi:10.1371/journal.pone.0029658.
- Schwarz, A. J., and McGonigle, J. (2011). Negative edges and soft thresholding in complex network analysis of resting state functional connectivity data. *Neuroimage* 55, 1132–1146. doi:10.1016/j.neuroimage.2010.12.047.
- Shannon, B. J., Dosenbach, R. A., Su, Y., Vlessenko, A. G., Larson-Prior, L. J., Nolan, T. S., et al. (2013). Morning-evening variation in human brain metabolism and memory circuits. *J. Neurophysiol.* 109, 1444–1456. doi:10.1152/jn.00651.2012.
- Šimonka, V., Fras, M., and Gosak, M. (2015). Stochastic simulation of the circadian rhythmicity in the SCN neuronal network. *Phys. A Stat. Mech. its Appl.* 424, 1–10. doi:<https://doi.org/10.1016/j.physa.2014.12.034>.
- Steel, A., Thomas, C., Trefler, A., Chen, G., and Baker, C. I. (2019). Finding the baby in the bath water – evidence for task-specific changes in resting state functional connectivity evoked by training. *Neuroimage* 188, 524–538. doi:<https://doi.org/10.1016/j.neuroimage.2018.12.038>.
- Storch, K.-F., Lipan, O., Leykin, I., Viswanathan, N., Davis, F. C., Wong, W. H., et al. (2002). Extensive and divergent circadian gene expression in liver and heart. *Nature* 417, 78–83. doi:10.1038/nature744.
- Susman, E. J., Dockray, S., Schiefelbein, V. L., Herwehe, S., Heaton, J. A., and Dorn, L. D. (2007). Morningness/eveningness, morning-to-afternoon cortisol ratio, and antisocial

- behavior problems during puberty. *Dev. Psychol.* 43, 811–822. doi:10.1037/0012-1649.43.4.811.
- Tassi, P., Pellerin, N., Moessinger, M., Eschenlauer, R., and Muzet, A. (2000). Variation of visual detection over the 24-hour period in humans. *Chronobiol. Int.* 17, 795–805. doi:10.1081/CBI-100102115.
- Telesford, Q. K., Joyce, K. E., Hayasaka, S., Burdette, J. H., and Laurienti, P. J. (2011). The Ubiquity of Small-World Networks. *Brain Connect.* 1, 367–375. doi:10.1089/brain.2011.0038.
- Trefler, A., Sadeghi, N., Thomas, A. G., Pierpaoli, C., Baker, C. I., and Thomas, C. (2016). Impact of time-of-day on brain morphometric measures derived from T1-weighted magnetic resonance imaging. *Neuroimage* 133, 41–52. doi:https://doi.org/10.1016/j.neuroimage.2016.02.034.
- Valdez, P., Ramírez, C., García, A., Talamantes, J., Armijo, P., and Borrani, J. (2005). Circadian rhythms in components of attention. *Biol. Rhythm Res.* 36, 57–65. doi:10.1080/09291010400028633.
- Valdez, P., Ramírez, and García, A. (2012). Circadian rhythms in cognitive performance: implications for neuropsychological assessment. *ChronoPhysiology Ther.* 2, 81–92. doi:10.2147/cpt.s32586.
- van den Heuvel, M. P., de Lange, S. C., Zalesky, A., Seguin, C., Yeo, B. T. T., and Schmidt, R. (2017). Proportional thresholding in resting-state fMRI functional connectivity networks and consequences for patient-control connectome studies: Issues and recommendations. *Neuroimage* 152, 437–449. doi:10.1016/j.neuroimage.2017.02.005.
- Vandewalle, G., Archer, S. N., Wuillaume, C., Balteau, E., Degueldre, C., Luxen, A., et al. (2009). Functional Magnetic Resonance Imaging-Assessed Brain Responses during an Executive Task Depend on Interaction of Sleep Homeostasis, Circadian Phase, and PER3 Genotype. *J. Neurosci.* 29, 7948–7956. doi:10.1523/JNEUROSCI.0229-09.2009.
- Vandewalle, G., Archer, S. N., Wuillaume, C., Balteau, E., Degueldre, C., Luxen, A., et al. (2011). Effects of Light on Cognitive Brain Responses Depend on Circadian Phase and Sleep Homeostasis. *J. Biol. Rhythms* 26, 249–259. doi:10.1177/0748730411401736.
- Vasalou, C., Herzog, E. D., and Henson, M. A. (2009). Small-World Network Models of Intercellular Coupling Predict Enhanced Synchronization in the Suprachiasmatic Nucleus. *J. Biol. Rhythms* 24, 243–254. doi:10.1177/0748730409333220.
- Vossel, S., Geng, J. J., and Fink, G. R. (2013). Dorsal and Ventral Attention Systems: Distinct Neural Circuits but Collaborative Roles. *Neurosci.* 20, 150–159. doi:10.1177/1073858413494269.
- Vyazovskiy, V. V., Cirelli, C., Pfister-Genskow, M., Faraguna, U., and Tononi, G. (2008). Molecular and electrophysiological evidence for net synaptic potentiation in wake and depression in sleep. *Nat. Neurosci.* 11, 200–208. doi:10.1038/nn2035.
- Wang, C., Song, S., d’Oleire Uquillas, F., Zilverstand, A., Song, H., Chen, H., et al. (2020). Altered brain network organization in romantic love as measured with resting-state fMRI

and graph theory. *Brain Imaging Behav.* doi:10.1007/s11682-019-00226-0.

Wang, J., Wang, L., Zang, Y., Yang, H., Tang, H., Gong, Q., et al. (2009). Parcellation-dependent small-world brain functional networks: A resting-state fMRI study. *Hum. Brain Mapp.* 30, 1511–1523. doi:10.1002/hbm.20623.

Wang, J., Zuo, X.-N. X., Gohel, S., Milham, M. P., Biswal, B. B., and He, Y. (2011). Graph theoretical analysis of functional brain networks: test-retest evaluation on short- and long-term resting-state functional MRI data. *PLoS One* 6, e21976. doi:10.1371/journal.pone.0021976.

Watts, D. J., and Strogatz, S. H. (1998). Collective dynamics of “small-world” networks. *Nature* 393, 440–442. doi:10.1038/30918.

Webb, A. B., Taylor, S. R., Thoroughman, K. A., Doyle III, F. J., and Herzog, E. D. (2012). Weakly Circadian Cells Improve Resynchrony. *PLOS Comput. Biol.* 8, e1002787. Available at: <https://doi.org/10.1371/journal.pcbi.1002787>.

Wilson, T. W., Heinrichs-Graham, E., and Becker, K. M. (2014). Circadian modulation of motor-related beta oscillatory responses. *Neuroimage* 102, 531–539. doi:<https://doi.org/10.1016/j.neuroimage.2014.08.013>.

Wu, Z., Pan, S., Chen, F., Long, G., Zhang, C., and Yu, P. S. (2020). A Comprehensive Survey on Graph Neural Networks. *IEEE Trans. Neural Networks Learn. Syst.*, 1–21. doi:10.1109/TNNLS.2020.2978386.

Yeo, B. T. T., Krienen, F. M., Sepulcre, J., Sabuncu, M. R., Lashkari, D., Hollinshead, M., et al. (2011). The organization of the human cerebral cortex estimated by intrinsic functional connectivity. *J. Neurophysiol.*

Zhang, J., Wang, J., Wu, Q., Kuang, W., Huang, X., He, Y., et al. (2011). Disrupted Brain Connectivity Networks in Drug-Naive, First-Episode Major Depressive Disorder. *Biol. Psychiatry* 70, 334–342. doi:<https://doi.org/10.1016/j.biopsych.2011.05.018>.

Appendix

Table A1. Summary of Shaefer/Yeo parcellation’s label name, component name, corresponding MNI coordinates, and the associated RGB code in the connectograms (7 networks, 200 nodes).

	Label name	Component name	MNI coordinates	RGB code
Visual Network (VN), Left Hemisphere				
1	LH_Vis_1	Visual	-24,-53,-9	123,104,238
2	LH_Vis_2	Visual	-26,-77,-14	147,112,219
3	LH_Vis_3	Visual	-45,-69,-8	138,43,226
4	LH_Vis_4	Visual	-10,-67,-4	201,160,220
5	LH_Vis_5	Visual	-27,-95,-12	204,204,255
6	LH_Vis_6	Visual	-14,-44,-3	75,0,130
7	LH_Vis_7	Visual	-5,-93,-4	181,126,220
8	LH_Vis_8	Visual	-47,-70,10	147,112,219

9	LH_Vis_9	Visual	-23,-97,6	167,107,207
10	LH_Vis_10	Visual	-11,-70,7	116,108,192
11	LH_Vis_11	Visual	-40,-85,11	138,43,226
12	LH_Vis_12	Visual	-12,-73,22	111,0,255
13	LH_Vis_13	Visual	-7,-87,28	120,81,169
14	LH_Vis_14	Visual	-23,-87,23	115,79,150

Somatomotor Network (SMN), Left Hemisphere

15	LH_SomMot_1	Somatomotor	-51,-4,-2	135,206,235
16	LH_SomMot_2	Somatomotor	-53,-24,9	30,144,255
17	LH_SomMot_3	Somatomotor	-37,-21,16	0,191,255
18	LH_SomMot_4	Somatomotor	-55,-4,10	0,0,205
19	LH_SomMot_5	Somatomotor	-53,-22,18	172,229,238
20	LH_SomMot_6	Somatomotor	-56,-8,31	135,206,250
21	LH_SomMot_7	Somatomotor	-47,-9,46	119,181,254
22	LH_SomMot_8	Somatomotor	-7,-12,46	79,134,247
23	LH_SomMot_9	Somatomotor	-49,-28,57	119,158,203
24	LH_SomMot_10	Somatomotor	-40,-25,57	65,102,245
25	LH_SomMot_11	Somatomotor	-31,-46,63	69,177,232
26	LH_SomMot_12	Somatomotor	-32,-22,64	49,140,231
27	LH_SomMot_13	Somatomotor	-26,-38,68	73,151,208
28	LH_SomMot_14	Somatomotor	-20,-11,68	15,192,252
29	LH_SomMot_15	Somatomotor	-5,-29,67	65,125,193
30	LH_SomMot_16	Somatomotor	-19,-31,68	0,127,255

Dorsal Attention Network (DAN), Left Hemisphere

31	LH_DorsAttn_Post_1	Posterior	-43,-48,-19	0,255,127
32	LH_DorsAttn_Post_2	Posterior	-57,-60,-1	50,205,50
33	LH_DorsAttn_Post_3	Posterior	-26,-70,38	173,255,47
34	LH_DorsAttn_Post_4	Posterior	-54,-27,42	144,238,144
35	LH_DorsAttn_Post_5	Posterior	-41,-35,47	60,179,113
36	LH_DorsAttn_Post_6	Posterior	-33,-49,47	34,139,34
37	LH_DorsAttn_Post_7	Posterior	-17,-73,54	152,255,152
38	LH_DorsAttn_Post_8	Posterior	-29,-60,59	144,238,144
39	LH_DorsAttn_Post_9	Posterior	-6,-60,57	119,221,119
40	LH_DorsAttn_Post_10	Posterior	-17,-53,68	116,195,101
41	LH_DorsAttn_FEF_1	Frontal Eye Fields	-31,-4,53	80,200,120
42	LH_DorsAttn_FEF_2	Frontal Eye Fields	-22,6,62	57,255,20
43	LH_DorsAttn_PrCv_1	Precentral Ventral	-48,6,29	34,139,34

Ventral Attention Network (DAN), Left Hemisphere

44	LH_SalVentAttn_ParOper_1	Parietal Operculum	-56,-40,20	249,132,229
45	LH_SalVentAttn_ParOper_2	Parietal Operculum	-61,-26,28	254,78,218
46	LH_SalVentAttn_ParOper_3	Parietal Operculum	-60,-39,36	207,113,175
47	LH_SalVentAttn_FrOperIns_1	Frontal Operculum Insula	-39,-4,-4	189,51,164
48	LH_SalVentAttn_FrOperIns_2	Frontal Operculum Insula	-33,20,5	204,0,204
49	LH_SalVentAttn_FrOperIns_3	Frontal Operculum Insula	-39,1,11	218,112,214
50	LH_SalVentAttn_FrOperIns_4	Frontal Operculum Insula	-51,9,11	241,167,254
51	LH_SalVentAttn_PFC1_1	Lateral Prefrontal Cortex	-28,43,31	238,130,238
52	LH_SalVentAttn_Med_1	Medial	-6,9,41	255,111,255
53	LH_SalVentAttn_Med_2	Medial	-11,-35,46	207,52,118
54	LH_SalVentAttn_Med_3	Medial	-6,-3,65	223,0,255

Limbic Network (LN), Left Hemisphere

55	LH_Limbic_OFC_1	Orbital Frontal Cortex	-24,22,-20	255,248,220
56	LH_Limbic_OFC_2	Orbital Frontal Cortex	-10,35,-21	240,230,140
57	LH_Limbic_TempPole_1	Temporal Pole	-29,-6,-39	252,247,94
58	LH_Limbic_TempPole_2	Temporal Pole	-45,-20,-30	255,250,205

59	LH_Limbic_TempPole_3	Temporal Pole	-28,10,-34	251,236,93
60	LH_Limbic_TempPole_4	Temporal Pole	-43,8,-19	255,247,0
Frontoparietal Network (FPN), Left Hemisphere				
61	LH_Cont_Par_1	Parietal	-53,-51,46	255,165,0
62	LH_Cont_Par_2	Parietal	-35,-62,48	255,140,0
63	LH_Cont_Par_3	Parietal	-45,-42,46	255,160,137
64	LH_Cont_Temp_1	Temporal	-61,-43,-13	255,200,124
65	LH_Cont_OFC_1	Orbital Frontal Cortex	-32,42,-13	255,153,102
66	LH_Cont_PFC1_1	Lateral Prefrontal Cortex	-42,49,-6	255,163,67
67	LH_Cont_PFC1_2	Lateral Prefrontal Cortex	-28,58,8	255,130,67
68	LH_Cont_PFC1_3	Lateral Prefrontal Cortex	-42,40,16	255,174,66
69	LH_Cont_PFC1_4	Lateral Prefrontal Cortex	-44,20,27	237,135,45
70	LH_Cont_PFC1_5	Lateral Prefrontal Cortex	-43,6,43	224,141,60
71	LH_Cont_pCun_1	Precuneus	-9,-73,38	255,153,51
72	LH_Cont_Cing_1	Cingulate	-5,-29,28	237,145,33
73	LH_Cont_Cing_2	Cingulate	-3,4,30	251,153,2
Default Mode Network (DMN), Left Hemisphere				
74	LH_Default_Temp_1	Temporal	-47,8,-33	240,128,128
75	LH_Default_Temp_2	Temporal	-60,-19,-22	255,69,0
76	LH_Default_Temp_3	Temporal	-56,-6,-12	165,42,42
77	LH_Default_Temp_4	Temporal	-58,-30,-4	255,0,0
78	LH_Default_Temp_5	Temporal	-58,-43,7	123,17,19
79	LH_Default_Par_1	Parietal	-48,-57,18	204,51,51
80	LH_Default_Par_2	Parietal	-39,-80,31	205,92,92
81	LH_Default_Par_3	Parietal	-57,-54,28	253,94,83
82	LH_Default_Par_4	Parietal	-46,-66,38	127,23,52
83	LH_Default_PFC_1	Prefrontal Cortex	-35,20,-13	255,53,94
84	LH_Default_PFC_2	Prefrontal Cortex	-6,36,-10	235,76,66
85	LH_Default_PFC_3	Prefrontal Cortex	-46,31,-7	204,78,92
86	LH_Default_PFC_4	Prefrontal Cortex	-12,63,-6	178,34,34
87	LH_Default_PFC_5	Prefrontal Cortex	-52,22,8	203,65,84
88	LH_Default_PFC_6	Prefrontal Cortex	-6,44,7	237,28,36
89	LH_Default_PFC_7	Prefrontal Cortex	-8,59,21	218,44,67
90	LH_Default_PFC_8	Prefrontal Cortex	-6,30,25	229,26,76
91	LH_Default_PFC_9	Prefrontal Cortex	-11,47,45	255,36,0
92	LH_Default_PFC_10	Prefrontal Cortex	-3,33,43	255,69,0
93	LH_Default_PFC_11	Prefrontal Cortex	-40,19,49	171,75,82
94	LH_Default_PFC_12	Prefrontal Cortex	-24,25,49	156,37,66
95	LH_Default_PFC_13	Prefrontal Cortex	-9,17,63	194,59,34
96	LH_Default_pCunPCC_1	Precuneus/Posterior Cingulate Cortex	-11,-56,13	196,30,58
97	LH_Default_pCunPCC_2	Precuneus/Posterior Cingulate Cortex	-5,-55,27	255,64,64
98	LH_Default_pCunPCC_3	Precuneus/Posterior Cingulate Cortex	-4,-31,36	211,0,63
99	LH_Default_pCunPCC_4	Precuneus/Posterior Cingulate Cortex	-6,-54,42	157,41,51
100	LH_Default_PHC_1	Parahippocampal Cortex	-26,-32,-18	205,92,92
Visual Network (VN), Right Hemisphere				
101	RH_Vis_1	Visual	39,-35,-23	123,104,238
102	RH_Vis_2	Visual	28,-36,-14	147,112,219
103	RH_Vis_3	Visual	29,-69,-12	138,43,226
104	RH_Vis_4	Visual	12,-65,-5	201,160,220
105	RH_Vis_5	Visual	48,-71,-6	204,204,255

106	RH_Vis_6	Visual	11,-92,-5	75,0,130
107	RH_Vis_7	Visual	16,-46,-1	181,126,220
108	RH_Vis_8	Visual	31,-94,-4	147,112,219
109	RH_Vis_9	Visual	9,-75,9	167,107,207
110	RH_Vis_10	Visual	22,-60,7	116,108,192
111	RH_Vis_11	Visual	42,-80,10	138,43,226
112	RH_Vis_12	Visual	20,-90,22	111,0,255
113	RH_Vis_13	Visual	11,-74,26	120,81,169
114	RH_Vis_14	Visual	16,-85,39	115,79,150
115	RH_Vis_15	Visual	33,-75,32	105,53,156

Somatomotor Network (SMN), Right Hemisphere

116	RH_SomMot_1	Somatomotor	51,-15,5	135,206,235
117	RH_SomMot_2	Somatomotor	64,-23,8	30,144,255
118	RH_SomMot_3	Somatomotor	38,-13,15	0,191,255
119	RH_SomMot_4	Somatomotor	44,-27,18	0,0,205
120	RH_SomMot_5	Somatomotor	59,0,10	172,229,238
121	RH_SomMot_6	Somatomotor	56,-11,14	135,206,250
122	RH_SomMot_7	Somatomotor	58,-5,31	119,181,254
123	RH_SomMot_8	Somatomotor	10,-15,41	79,134,247
124	RH_SomMot_9	Somatomotor	51,-22,52	119,158,203
125	RH_SomMot_10	Somatomotor	47,-11,48	65,102,245
126	RH_SomMot_11	Somatomotor	7,-11,51	69,177,232
127	RH_SomMot_12	Somatomotor	40,-24,57	49,140,231
128	RH_SomMot_13	Somatomotor	32,-40,64	73,151,208
129	RH_SomMot_14	Somatomotor	33,-21,65	15,192,252
130	RH_SomMot_15	Somatomotor	29,-34,65	65,125,193
131	RH_SomMot_16	Somatomotor	22,-9,67	0,127,255
132	RH_SomMot_17	Somatomotor	10,-39,69	0,191,255
133	RH_SomMot_18	Somatomotor	6,-23,69	29,172,214
134	RH_SomMot_19	Somatomotor	20,-29,70	25,116,210

Dorsal Attention Network (DAN), Right Hemisphere

135	RH_DorsAttn_Post_1	Posterior	50,-53,-15	0,255,127
136	RH_DorsAttn_Post_2	Posterior	52,-60,9	50,205,50
137	RH_DorsAttn_Post_3	Posterior	59,-16,34	173,255,47
138	RH_DorsAttn_Post_4	Posterior	46,-38,49	144,238,144
139	RH_DorsAttn_Post_5	Posterior	41,-31,46	60,179,113
140	RH_DorsAttn_Post_6	Posterior	15,-73,53	34,139,34
141	RH_DorsAttn_Post_7	Posterior	34,-48,51	152,255,152
142	RH_DorsAttn_Post_8	Posterior	26,-61,58	144,238,144
143	RH_DorsAttn_Post_9	Posterior	8,-56,61	119,221,119
144	RH_DorsAttn_Post_10	Posterior	21,-48,70	116,195,101
145	RH_DorsAttn_FEF_1	Frontal Eye Fields	34,-4,52	80,200,120
146	RH_DorsAttn_FEF_2	Frontal Eye Fields	26,7,58	57,255,20
147	RH_DorsAttn_PrCv_1	Precentral Ventral	52,11,21	34,139,34

Ventral Attention Network (VAN), Right Hemisphere

148	RH_SalVentAttn_TempOccPar_1	Temporal Occipital Parietal	57,-45,9	255,0,144
149	RH_SalVentAttn_TempOccParr_2	Temporal Occipital Parietal	60,-39,17	218,29,129
150	RH_SalVentAttn_TempOccParr_3	Temporal Occipital Parietal	60,-26,27	255,111,255
151	RH_SalVentAttn_PrC_1	Precentral	51,4,40	189,51,164
152	RH_SalVentAttn_FrOperIns_1	Frontal Operculum Insula	41,6,-15	189,51,164
153	RH_SalVentAttn_FrOperIns_2	Frontal Operculum Insula	46,-4,-4	204,0,204
154	RH_SalVentAttn_FrOperIns_3	Frontal Operculum Insula	36,24,5	218,112,214
155	RH_SalVentAttn_FrOperIns_4	Frontal Operculum Insula	43,7,4	241,167,254

156	RH_SalVentAttn_Med_1	Medial	7,9,41	255,111,255
157	RH_SalVentAttn_Med_2	Medial	11,-36,47	207,52,118
158	RH_SalVentAttn_Med_3	Medial	8,3,66	223,0,255
Limbic Network (LN), Right Hemisphere				
159	RH_Limbic_OFC_1	Orbital Frontal Cortex	12,39,-22	255,248,220
160	RH_Limbic_OFC_2	Orbital Frontal Cortex	28,22,-19	240,230,140
161	RH_Limbic_OFC_3	Orbital Frontal Cortex	15,64,-8	253,253,150
162	RH_Limbic_TempPole_1	Temporal Pole	30,9,-38	252,247,94
163	RH_Limbic_TempPole_2	Temporal Pole	47,-12,-35	255,250,205
164	RH_Limbic_TempPole_3	Temporal Pole	25,-11,-32	251,236,93
Frontoparietal Network (FPN), Right Hemisphere				
165	RH_Cont_Par_1	Parietal	62,-37,37	255,165,0
166	RH_Cont_Par_2	Parietal	53,-42,48	255,140,0
167	RH_Cont_Par_3	Parietal	37,-63,47	255,160,137
168	RH_Cont_Temp_1	Temporal	63,-41,-12	255,200,124
169	RH_Cont_PFCv_1	Ventral Prefrontal Cortex	34,21,-8	255,103,0
170	RH_Cont_PFCl_1	Lateral Prefrontal Cortex	36,46,-13	255,153,102
171	RH_Cont_PFCl_2	Lateral Prefrontal Cortex	29,58,5	255,163,67
172	RH_Cont_PFCl_3	Lateral Prefrontal Cortex	43,45,10	255,130,67
173	RH_Cont_PFCl_4	Lateral Prefrontal Cortex	46,24,26	255,174,66
174	RH_Cont_PFCl_5	Lateral Prefrontal Cortex	30,48,27	237,135,45
175	RH_Cont_PFCl_6	Lateral Prefrontal Cortex	41,33,37	224,141,60
176	RH_Cont_PFCl_7	Lateral Prefrontal Cortex	42,14,49	255,167,0
177	RH_Cont_pCun_1	Precuneus	14,-70,37	255,153,51
178	RH_Cont_Cing_1	Cingulate	5,-24,31	237,145,33
179	RH_Cont_Cing_2	Cingulate	5,3,30	251,153,2
180	RH_Cont_PFCmp_1	Medial Posterior Prefrontal Cortex	7,31,28	255,186,0
181	RH_Cont_PFCmp_2	Medial Posterior Prefrontal Cortex	7,25,55	228,155,15
Default Mode Network (DMN), Right Hemisphere				
182	RH_Default_Par_1	Parietal	47,-69,27	153,0,0
183	RH_Default_Par_2	Parietal	54,-50,28	228,113,122
184	RH_Default_Par_3	Parietal	51,-59,44	234,60,83
185	RH_Default_Temp_1	Temporal	47,13,-30	240,128,128
186	RH_Default_Temp_2	Temporal	61,-13,-21	255,69,0
187	RH_Default_Temp_3	Temporal	55,-6,-10	165,42,42
188	RH_Default_Temp_4	Temporal	63,-27,-6	255,0,0
189	RH_Default_Temp_5	Temporal	52,-31,2	123,17,19
190	RH_Default_PFCv_1	Ventral Prefrontal Cortex	51,28,0	255,64,64
191	RH_Default_PFCd/m_1	Dorsal/Medial Prefrontal Cortex	5,37,-14	220,20,60
192	RH_Default_PFCd/m_2	Dorsal/Medial Prefrontal Cortex	8,42,4	227,66,52
193	RH_Default_PFCd/m_3	Dorsal/Medial Prefrontal Cortex	6,29,15	215,59,62
194	RH_Default_PFCd/m_4	Dorsal/Medial Prefrontal Cortex	8,58,18	203,65,84
195	RH_Default_PFCd/m_5	Dorsal/Medial Prefrontal Cortex	15,46,44	255,83,73
196	RH_Default_PFCd/m_6	Dorsal/Medial Prefrontal Cortex	29,30,42	206,32,41
197	RH_Default_PFCd/m_7	Dorsal/Medial Prefrontal Cortex	23,24,53	232,0,13
198	RH_Default_pCunPCC_1	Precuneus/Posterior Cingulate Cortex	12,-55,15	196,30,58
199	RH_Default_pCunPCC_2	Precuneus/Posterior Cingulate Cortex	7,-49,31	255,64,64
200	RH_Default_pCunPCC_3	Precuneus/Posterior Cingulate Cortex	6,-58,44	211,0,63